PREDICTIVE SEMI-EMPIRICAL ANALYSIS FOR TIRE/SNOW INTERACTION

By

Naveen Kumar Sankapalli

RECOMMENDED:

Jonah Lee
Dr. Jonah Lee

Dr. Tinggang Zhang

Dr. Qing Liu

Chuen-Sen Lin
Dr. Chuen-Sen Lin, Advisory Committee Chair

Chair, Department of Mechanical Engineering

APPROVED:

John Aspnes
Interim Dean, College of Engineering and Mines

Dean of the Graduate School

January 6, 2005
Date

PREDICTIVE SEMI-EMPIRICAL ANALYSIS FOR TIRE/SNOW INTERACTION

A

THESIS

Presented to the Faculty
of the University of Alaska Fairbanks

in Partial Fulfillment of the Requirements
for the Degree of

MASTER OF SCIENCE

By
Naveen Kumar Sankapalli, B. Tech

Fairbanks, Alaska
December 2004

Abstract

A semi-analytical method is presented to predict the shear stress and motion resistance at the tire/snow interaction. The shear stress model is a function of normal pressure and slip. The main goal was to develop a simplified model by reducing the number of parameters in the model, so that the computational time could be reduced towards real time simulations. Motion resistance is calculated by integrating the horizontal component of normal pressure along the tire/terrain contact surface. The motion resistance obtained is slip dependent because the sinkage is a function of slip. The calculations of motion resistance and sinkage were done using the presented model and an existing model. Also the calculated results were compared with the FEA(Finite Element Analysis) data, which matched reasonably well. In the second part of the thesis shear force is expressed as a function of normal load, slip and slip angle. Shear force parameters tire stiffness, friction coefficients, and contact pressure constants were assumed as the functions of normal load and the coefficients of parameters were found through curve fitting using FEA data. These functions were used to calculate tire stiffness, friction coefficient and contact pressure constant. The calculated results matched well with FEA simulation results for the same tire and snow conditions. Pure shear force and the combined shear force were compared, and the pure shear force is always greater than the combined shear force for the same slip and slip angle.

Table of Contents

List of Figures

List of Tables

Acknowledgements

It gives me a great pleasure to thank all the individuals and research groups that supported me in this work. I would like to gratefully acknowledge the guidance and encouragement received from my advisor Dr. Chuen Sen Lin. I express my sincere thanks for his time and patience. I pay my sincere thanks to Dr. Qing Liu for helping me throughout my thesis. I also want to acknowledge my committee members Dr. Jonah Lee and Dr. Tinggang Zhang for their suggestions and valuable comments.

I am grateful to the Automotive Research Center for the financial support and encouragement extended through out this work.

Importantly, I want to thank my family members and friends for standing with me, providing moral support and encouraging me throughout my career.

1. Introduction

The performance of the vehicle as it travels over the unpaved terrain has become more significant nowadays as it has a wide range of applications, such as in construction projects, the petroleum industry, recreational activities, military operations, agriculture, etc. When the tire rolls over the terrain the performance of the vehicle depends on the terrain response. So it has become significant to know the terrain properties during the tire/terrain interaction. To determine the terrain behavior during off-road operations, the important task is to develop the pressure sinkage relationship and the shear stress-shear displacement relationship during the tire/terrain interaction. In developing these equations, it is not only important how accurately we develop these relationships but also how fast and conveniently these equations can be incorporated into the framework to predict the vehicle performance.

In cold regions, snow is the terrain with which many vehicles have to interact. At present we have little knowledge of the changing properties of snow and the movement of vehicles, as the mechanical properties of the snow are dependent on the pressure, temperature and time.

1.1 Objective

The main goal of this thesis is to develop a semi analytical model for shear stress as a function of normal pressure (σ_n) and slip (i) between the tire and terrain and apply this model to predict the performance of the vehicle on fresh snow. Slip is defined as distance that the tire travels when subjected to the driving torque that is less or greater than that in free rolling. The reason for developing this model is that the existing classic shear displacement model proposed by J. Y. Wong [1] contains many terrain properties such as cohesion modulus k_c, friction modulus k_ϕ, Bekker's exponent n, shear displacement modulus k, cohesion c, and friction angle ϕ. Hence this model is complicated in use for computation of the interface forces at the tire/terrain interaction. We planned to develop a semi-empirical shear stress model with a minimum number of constants and to reduce the computational time in the real time simulations of the vehicle.

We compared and performed parametric studies of the shear force in the pure and combined slip conditions (longitudinal and lateral directions).

1.2 Properties of Snow

Snow is the only solid that is slippery by nature because it is a non- homogeneous substance. It exists in three phases; the solid, liquid and gaseous states coexist at thermodynamic equilibrium, with composition corresponding to the pressure and temperature. Any change of pressure or temperature causes an immediate shift in the phase composition, thus involving fluctuations in the structure of the matter. Since snow is an aggregate of ice crystals and air, the factors involved in the phase change are particularly active. An increase in pressure and temperature between a sliding body and snow will invariably increase the amount of liquid phase, thereby providing the rubber surfaces with a lubricant, which considerably reduces the friction coefficient.

While dealing with soils we calculate the strength of the soil as a function of certain constants, like cohesion and internal friction angle of the soil. In the case of snow we also assumed that it is a type of cohesive and frictional mass [2]. This assumption may be little doubtful, as it depends upon the properties of the snow (i.e., the variability of cohesion and internal friction angle is more complex), because of the snow metamorphosis, which causes the state of the stress-strain relationship to depend on temperature, and because snow is more sensitive to the rate of load application. The shear strength of the snow depends on three factors: pressure, temperature and time [2].

1.3 Methods to Predict Wheel Performance over Snow

In this section we briefly discuss two mathematical models used to predict the vehicle performance over snow.

1. USATACOM-LLL method [3].
2. USAEWES method [3]

The terrain properties required for USATACOM-LLL [3] method are:

1. Plate sinkage tests for determining the pressure –sinkage relationship.
2. Shear stress-normal pressure tests for determining the shear deformation relationship.

The terrain properties required for the USAEWES [3] method are:

1. Cone index, to determine the soil penetration resistance at a certain depth.
2. Snow depth.

1.4 Approach

To evaluate the interface forces at the tire/terrain interface, the initial step is to determine the sinkage of the tire into snow due to the vertical load acting on the tire. Sinkage as a function of slip is calculated by numerically integrating the summation of vertical components of shear stress and normal pressure within the limits of zero sinkage and maximum sinkage, and subtracting the normal load, which is the weight of the vehicle. Here the shear stress is a function of sinkage and slip and the normal pressure is a function of sinkage; hence sinkage obtained is a function of slip. Wong's [4] pressure sinkage equation is substituted for obtaining the normal pressure. A semi-analytical shear stress model is developed, which is a function of normal pressure (σ_n) and slip (i) between the tire and the terrain, and it is applied for the sinkage calculation. The presented model is compared with the existing shear displacement model [4] for verification of the model. Motion resistance is calculated by integrating the horizontal component of normal pressure within the limits of zero sinkage and maximum sinkage. The second part of the thesis includes shear force calculations in terms of normal load, slip and slip angle, by expressing the shear force parameters, tire stiffness, friction coefficient, and contact pressure constants, in terms of normal load. Then the resultant shear forces due to pure and combined slip conditions are compared.

1.5 Overall View

In Chapter 2 we first discuss the calculations of the terrain characteristics using Bekkers model [4]. For this we used FEA (Finite Element Analysis) data [5] and through curve fitting obtained the Bekker's parameters. Then we discuss the two core models (TACOM & WES), which are mostly applied to obtain the interfacial forces at the tire/terrain interaction, and also briefly discuss the various motion resistance models.

In Chapter 3 we calculate shear force as a function of normal load, slip and slip angle. We express the shear force parameters tire stiffness, friction coefficient and contact pressure constants as a function of normal load through curve fitting using FEA

data. Then we compare the resultant shear force due to pure and combined slip conditions.

In Chapter 4 a semi-analytical shear stress model is developed and compared with the existing shear displacement model [4] for verification of the model. Then the new semi-analytical shear stress model is applied to obtain motion resistance, and compared with FEA data and results obtained from the existing shear displacement model [4].

2. Review of Tire/Snow Interaction Models

In off-road operation, we encounter various types of terrain with different behavior, ranging from desert sand through soft mud to fresh snow. The properties of the terrain quite often impose severe limitations to the mobility of off-road vehicles. So, we need to have adequate knowledge of the mechanical properties of the terrain, and its response to the vehicular loading, which is essential to the proper development and design of off-road vehicles for a given mission and environment.

In terramechanics the load, either wheel or track, is moving along the soil surface, and different approaches or methods have been developed in order to study the reactions of the terrain. Let us mention these methods briefly.

In the Bekker method [2] the soil constants are calculated from plate sinkage test results. The test arrangements and the analysis of the load-sinkage results are more complicated than in the WES method.

In the WES method [6] the soil penetration resistance is measured using a standard cone penetrometer. This is a rather simple operation, and the analysis of the load-sinkage results is easy.

The terrain which we are considering is fresh snow, which is assumed to be homogeneous and have a finite depth. The different pressure-sinkage models proposed by different authors and the identification of the constants are discussed in the next section.

2.1 Pressure Sinkage Models

2.1.1 Bekker's Pressure Sinkage Model and Identification of Constants

Bekker's pressure sinkage relationship for homogenous terrain is given as [7]

$$P = \left(\frac{k_c}{b} + k_\phi \right) z^n \tag{2.1}$$

Where

P -Normal Pressure

b -smaller dimension of the contact path,

k_c -cohesion modulus

k_ϕ -friction modulus

z -sinkage

n - Bekker's exponential

The constants k_c, k_ϕ, n can be obtained from a laboratory test conducted by Shoop [5].

The laboratory test pushed a 23-cm diameter rigid plate into a cube of snow 60*60*50 cm deep with an average initial density of approximately 200 kg/m^3. From the experimental curves of the laboratory test, using the MATLAB code, we extracted the numerical values of load vs. sinkage test data. Then by curve fitting the test data using the Bekker's equation, we found the values of k_c, k_ϕ, n. The values of fresh snow are found to be k_c= 3.43 kn/m^{n+1}; k_ϕ= 218.84215 kn/m^{n+2}; n=1.0707148 in SI units. From Figure 2.1 we can observe that the fitted curve and the experimental data matched well. The Figure 2.1 load-sinkage relationship obtained from the test is for infinite depth, because as the sinkage increases the normal load increases. So, we consider this data to determine the Bekker's constants.

Table 2.1 - Digitized laboratory test data reproduced from Figure 2.2

S:No	Sinkage(Meters)	Load(Newtons)	Pressure(kn / m^2)
1	0.02908805	126.86567164	3.053529
2	0.03262579	186.56716418	4.490508
3	0.03812893	223.88059701	5.388610
4	0.04834906	268.65671642	6.466332
5	0.05621069	402.98507463	9.699498
6	0.07311321	544.77611940	13.34219
7	0.07783019	634.32835821	15.26772
8	0.08647799	716.41791045	17.24353
9	0.09929078	880.95238095	21.203754
10	0.10354610	928.57142857	22.349903
11	0.10638298	988.09523810	23.782589
12	0.11914894	1142.85714286	27.507573
13	0.12411348	1178.57142857	28.367184
14	0.15390071	1261.90476190	30.372945
15	0.16524823	1321.42857143	31.805631
16	0.17588652	1357.14285714	32.665243
17	0.18652482	1535.71428571	36.963301
18	0.19148936	1642.85714286	39.542136
19	0.19858156	1726.19047619	41.547896
20	0.20212766	1857.14285714	44.699806

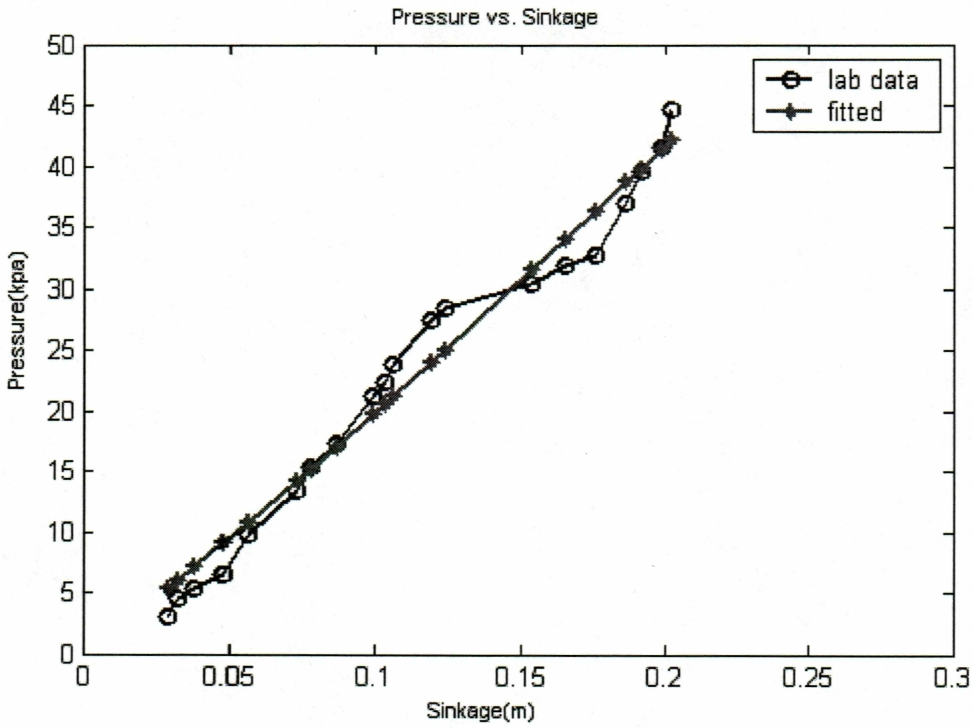

Figure 2.1 - Comparison of the fitted and experimental data

Figure 2.2 shows pressure-sinkage curves obtained using different areas of snow. We compared different snow terrains having different Bekker's constants [1, 3, 7, 8]. The curve, with Bekker's constants calculated through curve fitting using laboratory test data, indicates snow of infinite depth.

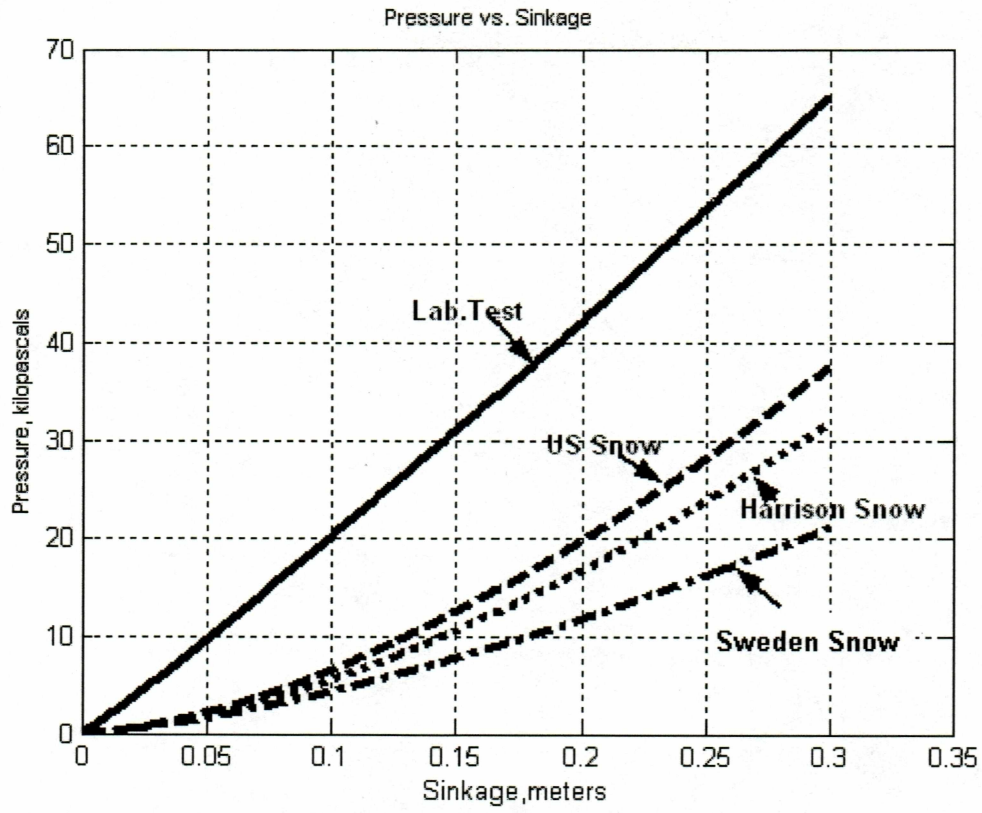

Figure 2.2 Pressure-sinkage curves obtained using different snows

2.1.2 Wong's Pressure Sinkage Equation

Wong [1,9 10] conducted experiments in Ontario and Canada. The pressure- sinkage data was obtained in a snow cover that contained a significant ice layer at a depth of approximately 10 cm (4 in) from the surface, with a snow ground at the base. The pressure first increases gradually with sinkage as the snow within a certain boundary under the plate is deformed. When the lower boundary of the deformation zone of the snow under the plate reaches the ice layer, the pressure increases rapidly with increase in the sinkage. When the applied pressure exceeds a certain level, the ice layer is broken, resulting in sudden drop in pressure. After the ice layer is fractured, further penetration of the plate produces increasing deformation of the snow beneath the ice layer. As the plate approaches the frozen ground at the base of the snow cover, the pressure again increases rapidly, and the pressure sinkage curve approaches an asymptote. Based on these

behaviors the pressure-sinkage relationship, before as well as after the failure of the ice layer, may be described by an exponential function of the following form [1, 9, 10]

$$z = z_w\left[1-\exp\left(-\frac{\sigma_n}{p_w}\right)\right] \tag{2.2}$$

or

$$\sigma_n = p_w\left[-\ln\left(1-\frac{z}{z_w}\right)\right] \tag{2.3}$$

Where

σ_n -pressure

z -sinkage

z_w -defines the asymptote of the pressure–sinkage curve and in the first approximation may be taken as the depth of the ice layer or that of the frozen ground .

p_w -is an empirical parameter which may be taken as 1/3 of the pressure where the sinkage z is 95% of the value of z_w.

2.1.3 Reece Pressure Sinkage Equation

Reece[11] has proposed a new equation for the pressure-sinkage relationship, given by

$$\sigma_n = \left(ck_c^{'} + \gamma_s b k_\phi^{'}\right)\left(\frac{z}{b}\right)^n \tag{2.4}$$

where

n, $k_c^{'}$ and $k_\phi^{'}$ are the pressure sinkage parameters

γ_s-weight density of the terrain

c -cohesion

A number of experiments were conducted to verify the validity of the equation (2.4). Reece pointed out that that equation (2.4) differs from equation (2.1) in the effect of the width, which is sufficient to mark a radical improvement. The soil values in the equation

(2.4) $k_c^{'}, k_\phi^{'}$ are dimensionless, whereas k_c, k_ϕ in the equation (2.1) have a variable dimension depending on the value of n. The equation (2.4) applies only for homogeneous soils and for non-homogeneous soils the pressure-sinkage relationship obtained using a smaller size plate may not be extrapolated to that of the larger-size contact area. This is because, for the same ratio of z/b, a plate with larger dimension b has to penetrate to a deeper layer of the terrain, which may have different mechanical properties from those of a shallower layer. The pressure-sinkage tests were also carried out using a Swiss Rammsonde with a cone base diameter of 100 mm [12].

In the next section we will discuss the different failure criteria of the terrain postulated by different authors.

2.2 Mohr-Coloumb Shear Stress Model

Soil shear strength is of prime importance when developing thrust models for estimating the mobility. The soil deformation modulus in connection with shear strength, permits development of slip models for tire-soil interaction.

The shear strength of the soil follows the classical Coulomb's formula as [1,13]

$$\tau = c + \sigma_n \tan\phi \tag{2.5}$$

where

τ- shear strength, kPa

c -soil cohesion, kPa

σ_n -normal pressure kPa

ϕ - soil internal friction,

In pure cohesion soils (ϕ=0) the shear strength consists of cohesion only, and in pure friction soils (c=0) the soil strength depends on soil internal friction angle (ϕ) and the normal pressure. Soil internal friction angle can be estimated based on soil compaction degree, granulometry and particle forms [2].

When dealing with soil, it has been assumed that its strength may be determined as a function of certain 'constants', which are called friction ϕ, cohesion c, and specific gravity, γ [2]. These are quite sufficient to generate and to establish an approximate and

general theory of soil power in supporting certain types of loads. Snow is also assumed to be another type of cohesive and frictionless mass, but this assumption is doubtful because of the ever-changing properties of snow [38]. The constants for cohesion and friction are to be treated in a similar way in the case of the snow. Certainly in this case the variability of c and ϕ is more complex, because of the snow metamorphosis that causes the state of stress relationship to depend on temperature, and because the variability is more sensitive to the rate of load application.

Experiments [2] made on the shear strengths of various materials indicate that the equation (2.5) is satisfied practically without exception, and that the line of rupture obtained experimentally for materials like marble, concrete and soil is the straight line corresponding to equation (2.5).

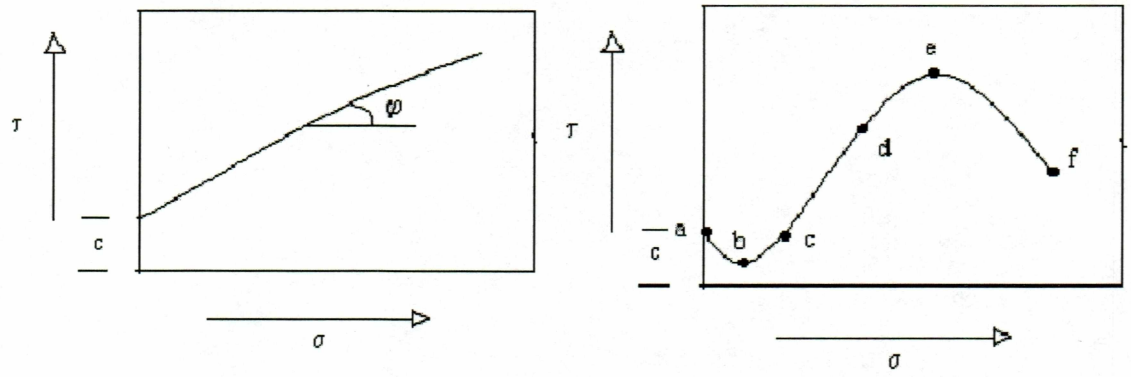

(a) For Soil (b) For Snow

Figure 2.3. Shear stress vs. normal pressure for soil and snow [2].

Figure 2.3a shows the Mohr-Coloumb failure criteria for soil, marble, and concrete. Figure 2.3b shows the Mohr Coloumb failure criteria for fresh snow at constant temperature. However, similar lines determined experimentally for snow have a different character and are far from satisfying the equation, since the shearing strength of the snow is a function of at least three independent factors: pressure, time and temperature. If temperature is kept constant, the relationship between τ and σ_n will be as shown in

Figure 2.3b. A fresh snow sample subjected to pressure σ_n undergoes a disruption of its structure, which is followed by a decrease in the τ line (a-b). When the pressure is further increased an increase in τ will be observed. This phenomenon may be explained by the effect of compaction and changes in snow structure, expressed by the solidification line (b-c-d). Further compression leads to the changing of snow into ice, the strength of which (point e) finally yields into a plastic flow up to point F, from which a complete liquefaction may end the process. The lower the temperature, the higher is the value of e. The line of rupture of snow a-b-c-d-e-f cannot be represented, therefore, by the equation (2.5), though at a particular instant, it may be interpreted as a certain function of the variable 'constants' c and ϕ. Experiments [2] indicate that the process described by the line a-b-c in Figure 2.3b has a little practical importance from the point of view of vehicle operation, because it refers to very low pressures, which can never be attained in vehicle design. However, within the range of pressures encountered, the line c-d-e is representative for the types of snow so far tested, in conjunction with vehicle performance. The results of the experiments, which lead to this conclusion, are shown in Figure (2.4).

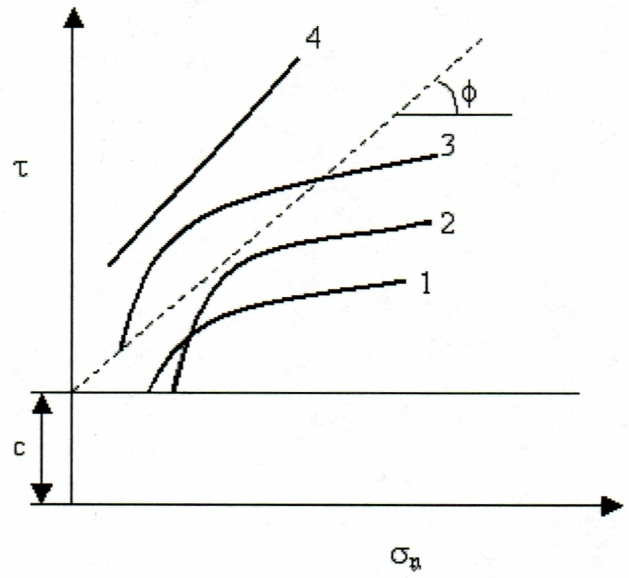

Figure 2.4. Experimental results of shear stress vs. normal pressure for snow

Various types of snow, designated by the numbers 1, 2, 3 and 4, produce almost a straight-line relationship between τ and σ_n, which relates to pressure enclosed between 1 and 4 psi [2]. This relationship corresponds to that expressed by the line c-d-e of the general curve shown in Figure 2.3b. Thus it appears possible to determine snow shear in any specific case. Under this assumption equation (2.5), used to determine the shear strength is valid when referred to snow. The application of the general methods similar to those used in soil mechanics, for the purpose of determining the state of stress in a snow cover, appear to be justified.

2.3 Tire/Snow Interaction Models

In this section we will discuss the two methods that predict wheel performance on shallow snow.

2.3.1 Land Locomotion Laboratory Method (LLL) or USATACOM Method

The technique for determining the terrain properties using the plate sinkage test was proposed by Bekker [7]. This technique is also called the bevameter technique. In this test a plate of suitable size is used to simulate the contact area of the vehicle running

gear, and the pressure sinkage relationship of the terrain is measured. This test is used to determine the pressure distribution at the tire terrain interface. The size of the plate should be compatible with that of the contact area of the tire/terrain interface, in order to minimize the uncertainty in applying the measured data to the prediction of the performance of the real vehicle.

The alternate method proposed by Wong [1, 9, 10] for specifying the pressure-sinkage relationship is depth dependent. In this thesis our area of interest is fresh shallow snow, which is defined as the snow where the 'pressure bulb' (i.e. the snow compacted due to the weight of the vehicle) intersects a rigid interface [8]. Since this is the case of the finite depth, we use Wong's [1, 9, 10] pressure-sinkage relationship to determine the sinkage of the snow. Several analytical models have been developed to predict the tractive performance of the rigid wheel on soft terrain [1, 15, 48]. To evaluate the relation between the tractive effort and slip of the rigid wheel, the development of shear displacement along the wheel-snow interface has to be determined. The shear displacement developed along the contact area of the rigid wheel may be determined based on the analysis of the slip velocity V_j as shown in Figure 2.5. The absolute speed of a point on the circumference of the wheel can be determined by the wheel speed, radius and angular velocity [14]. For a rigid wheel, the tangential component V_j of the absolute velocity of a point on the rim defined by the angle θ can be expressed by [15]

$$V_j = r\, w[1-(1-i)\cos\theta] \tag{2.6}$$

where

r -radius of wheel

w -angular velocity of wheel

i - slip of wheel

From equation (2.10) we can say that the slip velocity for the rigid wheel varies with the angle θ and slip.

The shear displacement along the wheel soil interface is defined by [15]

$$j = \int_0^t V_j dt = \int_{\theta}^{\theta_0} rw[1-(1-i)\cos\theta]\frac{d\theta}{w}$$

$$= r[(\theta_0 - \theta) - (1-i)\cdot(\sin\theta_0 - \sin\theta)] \tag{2.7}$$

Where

θ_0 is the entry angle that defines the angle measured from wheel centerline to a point on the rim that comes into contact with the terrain.

In order to improve the accuracy some researchers have measured the soil deformation by conducting experiments [49]. The shear stress distribution along the contact area can be determined by the equation [1, 7, 16]

$$\tau_x = [c + \sigma_n \tan\varphi]\cdot\left(1 - e^{\frac{-j}{k}}\right)$$

$$= [c + \sigma_n \tan\phi]\cdot\left(1 - e^{\frac{-r}{k}[\theta_0 - \theta - (1-i)(\sin\theta_0 - \sin\theta)]}\right) \tag{2.8}$$

By integrating the horizontal component of the tangential stress over the entire contact area, the total tractive effort F can be determined [1, 15]

$$F = \int_0^{\theta_0} \tau_x \cos\theta \, d\theta \tag{2.9}$$

The drawbar pull is given by the equation [1, 15,17]

$$F_d = rb\left[\int_0^{\theta_0} \tau_x \cos\theta \, d\theta - \int_0^{\theta_0} \sigma_n \sin\theta \, d\theta\right] \tag{2.10}$$

The vertical load is given by the equation [1, 15]

$$W = rb\left[\int_0^{\theta_0} \tau_x \sin\theta \, d\theta + \int_0^{\theta_0} \sigma_n \cos\theta \, d\theta\right] \tag{2.11}$$

The wheel torque is given by the equation [1, 15]

$$M_W = r^2 b \int_0^{\theta_0} \tau(\theta) d\theta \tag{2.12}$$

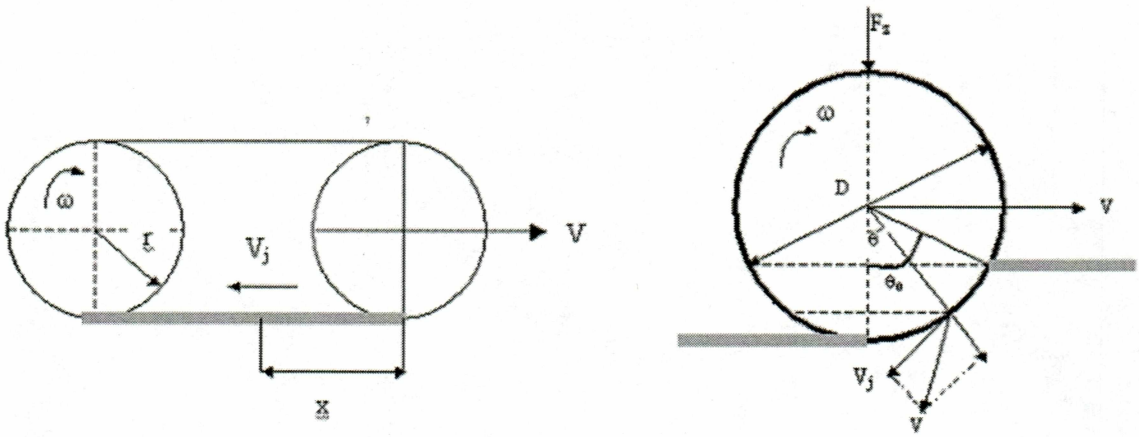

Figure 2.5 Shear displacement under the wheel

2.3.2 Waterways Experiment Station (WES) Method

To determine the vehicle performance using the WES method [6] the terrain properties are characterized by cone index, obtained using a cone penetrometer. WES developed an empirical equation relating Bekker's parameters to cone index [18]. Cone index is the force per unit cone base area and its units are pressure. The commonly used cone penetrometer consists of a 30° circular cone with a 0.5 in^2 base area, a proving ring and dial gauge for indicating the force required to push the cone into the terrain. The rate of penetration is approximately 12 in/sec [19]. This cone index is used to determine the dimensionless quantity, wheel numeric, and then mobility index is calculated. Based on the wheel numeric the tire performance parameters like drawbar coefficient and traction coefficient are calculated. The different wheel numeric models are described in the next section.

In this WES method [6] two types of dimensionless parameters are used. The vehicle mobility is described using mobility parameters and the wheel soil interaction using the wheel numeric, which is based on wheel characteristics and the CI-value (cone index) of the soil. Figure 2.7 shows the free-body diagram of NRMM-II simple force analysis.

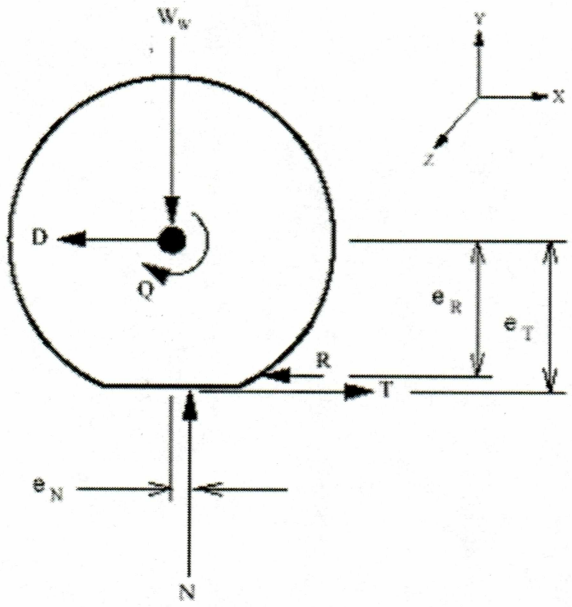

Figure 2.6 Free body diagram of NRMM-II simple force analysis [6]

e_N-eccentricity of normal force

e_R-eccentricity of resistance force

e_T-eccentricity of tractive force

R-motion resistance force from soil

Q-torque from power train

T-traction force from soil

N-normal force from soil.

W_w-wheel load from axle

D-draw bar pull from axle

Now let us discuss the mobility parameter, which is a simple means to access vehicle mobility on a "go/ no go" basis on different terrain. Pull coefficient or net traction coefficient, and drawbar pull coefficient are related by

$$\mu_p = \frac{P}{w} \tag{2.13}$$

where

μ_p–net traction coefficient

P-drawbar pull

w-wheel load

The rolling resistance coefficient or towed force coefficient is given by

$$\mu_r = \frac{P_r}{w} \tag{2.14}$$

where

μ_r - rolling resistance coefficient

P_r - rolling resistance, resistance to movement

w - wheel load KN

The thrust coefficient or gross traction coefficient or traction coefficient is given by

$$\mu_t = \frac{Q}{r_r.W} \tag{2.15}$$

where

μ_t – thrust coefficient (gross) traction coefficient

r_r - rolling radius of the wheel

Q - wheel torque, KNm

W -wheel load, KN

The different kinds of wheel numerics (used to find the mobility of the vehicle) that are proposed by different authors [20-29,50] differ mainly in the tire width and tire deflection factors. The original dimensionless wheel numerics were given in equation [6]

$$\frac{P}{w}, \frac{P_r}{w}, \frac{Q}{r_r.W} = f\left[\frac{CI.b.d}{W}, S, \frac{b}{d}, \frac{\delta}{h}\right] \tag{2.16}$$

Where the wheel and the soil variables are defined below

CI – cone index, soil penetration at a certain depth

b - tire section width, m

d - tire diameter, m

W - tire load, KN

S – slip

δ - tire deflection

h - tire section height, m

Brixius [24] proposed the wheel numeric given by

$$N_B = \frac{CI \cdot b \cdot d}{W} \cdot \left(\frac{1+5 \cdot \frac{\delta}{h}}{1+3 \cdot \frac{b}{d}} \right) \tag{2.17}$$

The Brixius [24] models are based on the farm tractor draw pull tests carried out by John Deere Co. in the USA

$$\mu_T = 0.88 \cdot (1 - e^{-0.1 N_B}) \cdot (1 - e^{-0.75 \cdot S}) + 0.04 \tag{2.18}$$

$$\mu_P = 0.88 \cdot (1 - e^{-0.1 \cdot N_B}) \cdot (1 - e^{-0.75 \cdot S}) - \left(\frac{1.0}{N_B} + \frac{0.05 \cdot S}{\sqrt{N_B}} \right) \tag{2.19}$$

$$\mu_R = \frac{1.0}{N_B} + 0.04 + \frac{0.05 \cdot S}{\sqrt{N_B}} \tag{2.20}$$

2.3.3 K. A. Abd El-Gawwad et al. Model

Gawwad and Crolla [30-33] have modified Bekker's model of the pressure–sinkage relationship and, also, the shear stress-shear displacement relationship. They assumed the tire/terrain contact area had two sections, the loading section and the unloading section. For the loading section they used Bekker's pressure–sinkage relationship. For the unloading section the predicted normal pressure distribution is as follows

$$p = \left(\frac{k_c}{b} + k_\phi \right) z_u^{\ n} - k_u (z_u - z) \tag{2.21}$$

Where

$k_u = k_0 + A_u z_u$

z_u is the sinkage when unloading begins

k_0 and A_u are parameters whose values are determined from the experimental data.

In determining the shear stress as a function of shear displacement for pneumatic tires they introduced a constant J_o, which accounts for the fact that a threshold perimeter shear exists at which the movement of the wheel starts. Thus the equation has been modified as follows:

$$\tau = (c + \sigma_n \tan\phi)(1 - e^{-(j+j_0)/k}) \tag{2.22}$$

The slip-shear parameters, J_o and k, not only depend on the soil properties but also on tire characteristics and the applied load. The following relationships are proposed for the determination of the slip-shear parameters, for cohesive soils based on tire tests in clay:

$$j_0 = -0.065+0.49/\text{MOBN}$$

$$k = -0.06+0.66/\text{MOBN}$$

Where

MOBN is the mobility number.

2.3.4 Yukio Nikajima Model

Yukio Nikajima [34] developed an analytical model to estimate the longitudinal traction of the tire on the snow. The model consists of four kinds of forces: braking force attributable to snow compression, shear force of snow in void (space between tread blocks), frictional force, and digging force (edge effects generated by sipes and blocks) [35]. The mechanical characteristics of snow were considered in the prediction of the braking force and shear force, but were not considered in the prediction of other forces. The contribution of shear force of snow in void and the frictional force was large in static friction and the digging force and frictional force were large in case of high slip ratios.

2.4 Different Motion Resistance Models

2.4.1 Richmond's Model

Richmond [36, 37] has developed an empirical equation for motion resistance. This empirical equation is applicable to a large range of vehicles, both wheeled and tracked, and does not require many elaborate measurements of snow properties. The vehicle is installed with load cells on all four wheels and these load cells measure the longitudinal, vertical and lateral forces at the tire/terrain interface. Longitudinal forces represent the net traction or motion resistance depending on whether the tire is driven or free rolling. The resistance forces are measured at all four wheels by towing the vehicle.

The snow and tire characteristic dimensions are shown in Figure 2.8

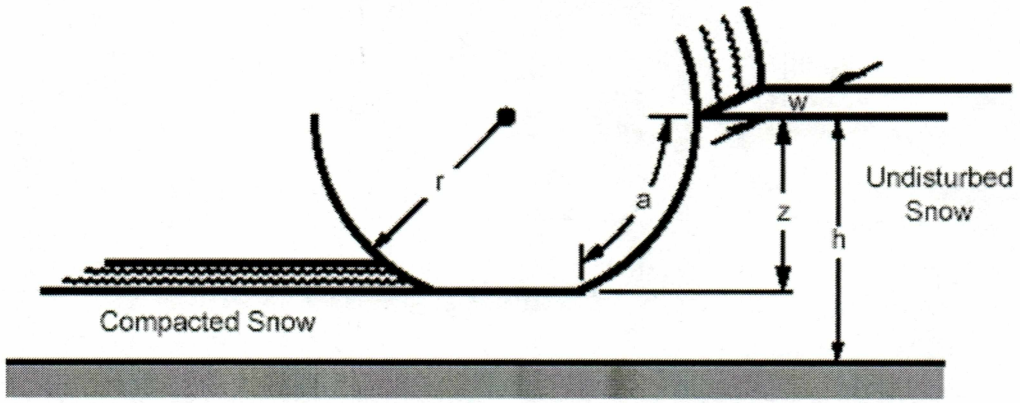

Figure 2.7 Snow and tire characteristic dimensions [37]

Using all data a new equation is obtained for motion resistance, which is given by [37,38]

$$R_s = 21.313(\rho_0 aw)^{1.1918} \tag{2.23}$$

Where

ρ_0 - the average initial undisturbed density of the snow,

a - the arc length of the tire in contact with the snow,

w -the maximum tire width in meters.

2.4.2 Bekker's Model

Bekker [4] has proposed a method to predict the motion resistance of the rigid wheel. In this method he has made the assumption that the terrain reaction at all the points on the contact surface is purely radial, and is equal to the normal pressure beneath a horizontal plate at the same depth in the pressure sinkage test.

The equation in terms of the wheel sinkage is given by

$$R_c = b\left[\left(\frac{k_c}{b} + k_\varphi\right) \cdot \frac{z_0^{n+1}}{n+1}\right] \tag{2.24}$$

Where

R_c is the motion resistance, which is the work done per unit length in pressing a plate of width b into the ground of depth z_0.

In order to express the sinkage in the above equation in terms of terrain and the tire characteristics, Bekker has proposed the following equation [4]

$$R_c = \frac{1}{(3-n)^{(2n+2)/(2n+1)}(n+1)b^{1/(2n+1)}\left(\frac{k_c}{b}+k\varphi\right)^{1/(2n+1)}} \cdot \left[\frac{3W}{\sqrt{D}}\right]^{(2n+2)/(2n+1)} \tag{2.25}$$

According to the above theory the maximum normal pressure should occur at the lowest point of the contact where the sinkage is maximum, but experiments show that the maximum normal pressure should occur at the bottom dead center and its location varies with slip [39].

2.4.3 Gerard W. H. VanEs Model

Gerard W. H. VanEs [40] predicted the rolling resistance of aircraft tires in dry snow. These predicted empirical equations have much better agreement with the experimental results. The total rolling resistance of an aircraft tire rolling along snow-covered runway is given by

$$D_{rolling} = D_r + D_c + D_d \tag{2.26}$$

Where

D_r -rolling resistance on dry hard surface

D_c - the compaction resistance given by the equation

$$D_c = \frac{b\sigma_i\rho_0 h_0}{\rho_i\sqrt{\lambda}}\int_{u_f}^{u_0} e^{-u^2}du$$

Where

$$u_0 = \sqrt{\lambda}\left(\frac{\rho_i}{\rho_0}-1\right) \qquad u_f = \sqrt{\lambda}\left(\frac{\rho_i}{\rho_f}-1\right)$$

r-void ratio defined as the ratio of the void volume to the volume of the solid ice grains.

$$r = \frac{\rho_i}{\rho}-1$$

ρ_i -density of ice

ρ-actual snow density

ρ_0-initial snow density

ρ_f-final snow density of snow after compression

h_0-initial snow depth

b-effective tire width at the point of contact between tire and snow surface

λ-grain structure index varies from 1 to 2; for natural snow its value is 1

2.5 Summary

Now let us summarize all the theories discussed in the previous sections. We have basically two models, TACOM and WES, to determine the tire/terrain interaction forces of the vehicle over the off-road terrain. In the TACOM method we need to have the pressure sinkage curves, and the shear test to determine the tire and the terrain characteristics. In this method we have many disadvantages. For example, for non-homogenous terrain the curve may not behave exponentially (according to Bekker's assumption), and for snow the behavior of the curve may depend on the temperature, density, depth, etc. For these reasons we may not get the accurate tire/terrain characteristics, which are used as the input values to determine the interface forces at the tire/terrain interaction.

In the WES method we need to perform the cone index test, which is easier than Bekker's pressure–sinkage test, to determine the characteristics of the tire/terrain interaction. This method gives better results than the TACOM method. In this method we do not require the shear test. In this method the number of parameters are less than the number of parameters involved in the TACOM method, in determining the tire/terrain characteristics. So the WES method is the better method to determine the vehicle mobility.

These methods also have limitations; for instance, their usefulness in the development of new vehicle design concepts or in the prediction of vehicle performance in new operating environments is uncertain. Furthermore, an entirely empirical approach is only feasible where the number of variables involved in the problem is relatively small. If large numbers of variables are required to define the problem, then an empirical approach may not be cost effective.

In this thesis TACOM methodology is used and a simplified semi-analytical model is developed to determine the interface forces (i.e. traction force, motion resistance) at the tire/terrain interaction. The presented shear stress model is a simplified model with fewer parameters, so that the computational time could be reduced toward real time simulations. The tire/terrain characteristics are determined using Wong's pressure sinkage model and Mohr-Coloumb failure criteria.

3. Parametric Analysis of Shear Forces

This chapter deals with the comparison of the pure and combined shear forces at the tire/terrain interaction. The external forces generated at the tire/terrain interface, when the vehicle moves in an arbitrary direction, are the lateral and longitudinal forces. In defining pure shear force we have two cases, pure longitudinal force and pure lateral force. Pure longitudinal force is the special case of the combined force, in which the slip angle is zero. Pure lateral force is the case in which the slip is zero. The term pure force used in this study is the vectorial sum of pure longitudinal force and pure lateral force. In defining combined shear force [41] we have two cases, combined longitudinal force and combined lateral force. Combined longitudinal force is the shear force with both slip and slip angle in the longitudinal direction. The term combined shear force used in this study is the vectorial sum of combined longitudinal force and combined lateral force.

The shear force is a function of tire stiffness, friction coefficient, and contact pressure constant. Our goal is to express these parameters as functions of normal load and formulate these functions using a minimum number of coefficients. These coefficients are constants and are derived from curve fitting using FEA data [5, 42]. Parametric analysis was done in order to observe the behavior of shear force with respect to change of tire stiffness, friction coefficient, and the contact pressure constants.

The next section discusses the definitions of each of the parameters in detail.

3.1 Definitions

Braking and driving slip:

The generalized longitudinal slip is given by

$$S_x = \frac{V_x - \omega r}{\omega r} \tag{3.1}$$

The braking and driving slips are defined as

$$S_d = \frac{\omega r - V_x}{\omega r} \tag{3.2}$$

$$S_b = \frac{V_x - \omega r}{V_x} \tag{3.3}$$

Where

S_x-longitudinal slip

V_x- linear speed of the tire center

ω-Angular speed of the tire

r-rolling radius of the free rolling tire

The relationship between driving and braking slip is given by

$$S_x = -S_d \; ; \; S_x = \frac{S_b}{1-S_b} \text{ or } \quad S_b = \frac{S_x}{1+S_x} \tag{3.4}$$

Combined friction coefficient:

When a vehicle is moving, if the brake is applied suddenly and the steering wheel is turned, then the wheel may experience friction force which is the result of both, the longitudinal friction coefficient μ_x, and the lateral friction coefficient μ_y [43].

Let μ_x and μ_y be the friction coefficients along the longitudinal and lateral directions. The combined friction coefficient is neither the resultant nor the average of the longitudinal and lateral friction coefficient equations. The reason is that the friction coefficients are non-linear functions of normal force.

$$\mu_\Sigma \neq \sqrt{\mu_x^{\,2} + \mu_y^{\,2}} \tag{3.5}$$

$$\mu_\Sigma \neq \frac{\mu_x + \mu_y}{2} \tag{3.6}$$

So to compute the combined friction coefficient, μ_Σ, two non dimensional quantities are introduced, which are termed the normalized slip along the longitudinal and lateral directions which are discussed in detail in the next section.

Normalized slip:

Let ϕ_x be the normalized longitudinal slip which is given by [44]

$$\phi_x = \frac{C_s S_x}{\mu_x F_z} \tag{3.7}$$

Where

C_s-longitudinal tire stiffness [45] $C_s = \left.\frac{\partial F_x}{\partial s_x}\right|_{s_x=0}$

S_x-longitudinal slip

μ_x-longitudinal friction coefficient

F_z –normal load

F_x –longitudinal Force

Let ϕ_y be the normalized lateral slip, which is given by [44]

$$\phi_y = \frac{C_\alpha (1 + S_x) \tan \alpha}{\mu_y F_z} \tag{3.8}$$

C_α-lateral tire stiffness and $C_\alpha = \left. \frac{\partial F_y}{\partial \alpha} \right|_{\alpha=0}$

S_x-longitudinal slip

α - slip angle

F_z –normal load

μ_y-lateral friction coefficient

F_y – lateral Force

The normalized combined slip is given by

$$\phi = \sqrt{\phi_x^{\,2} + \phi_y^{\,2}} \tag{3.9}$$

ϕ-normalized combined slip

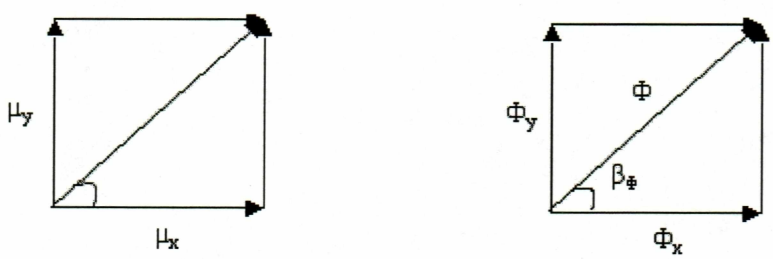

Figure 3.1 Friction coefficients and normalized slips along the longitudinal and lateral directions

Shear distribution equation:

Let $N(\phi)$ be the normalized shear force[46], which when multiplied by the original function equations (3.11 – 3.16) produce the interactive effect of slip on lateral force and slip angle on longitudinal force. When the tire operates only with slip or slip angle, the normalized shear force takes the value of one. The normalized shear force takes the form of equation (3.10)

$$N(\phi)=1-\exp\left(-\phi-E_1\phi^2-E_2\phi^3\right) \tag{3.10}$$

The first order contact pressure constant E_1 is related to second order contact pressure constant E_2 as

$$E_2=E_1^{\,2}+1/12$$

The boundary conditions [46] of the equation (3.10) are given in Table(3.1).

Table 3.1 Boundary conditions of normalized shear force equation

	ϕ=0	ϕ=+∞
$N(\phi)$	0	1
$dN(\phi)/d\phi$	+1	0
$dN^2(\phi)/d^2\phi$	$2E_1$-1≤0	N/A
$dN^3(\phi)/d^3\phi$	$0 \le 6(E_2-E_1)+1 \le 1.5$	N/A

At $dN^2(\phi)/d^2\phi = dN^3(\phi)/d^3\phi=0$ the contact pressure is almost uniform.

The pure longitudinal shear force $F_x\big|_{\alpha=0}$ is defined as the shear force with zero slip angle.

$$F_x\big|_{\alpha=0}=\mu_x F_z N(\phi_x) \tag{3.11}$$

The pure lateral shear force $F_y\big|_{s_x=0}$ is defined as the lateral force with zero slip (S_x=0).

$$F_y\big|_{S_x=0}=\mu_y F_z N\left(\phi_y\big|_{s_x=0}\right) \tag{3.12}$$

The vector sum of pure shear forces is given by the equation (3.13).

$$F_{pure} = \sqrt{F_x^{\,2}\big|_{\alpha=0} + F_y^{\,2}\big|_{s_x=0}} \tag{3.13}$$

The combined longitudinal shear force $F_x\big|_{\alpha\neq 0}$ is defined as the longitudinal component of shear force with non-zero slip and slip angle ($\alpha\neq 0$, $S_x\neq 0$).

$$F_x\big|_{\alpha\neq 0} = \mu_x F_z N(\phi)\cos\beta_\phi \tag{3.14}$$

The combined lateral shear force $F_y\big|_{s_x\neq 0}$ is defined as the lateral component of shear force with non-zero slip and slip angle ($\alpha\neq 0$, $S_x\neq 0$). This is the component of the combined shear force in the lateral direction.

$$F_y\big|_{S_x\neq 0} = \mu_y F_z N(\phi)\sin\beta_\phi \tag{3.15}$$

The resultant of the two is called combined shear force and is given by equation (3.16)

$$F_\Sigma = \mu_\Sigma F_z N(\varphi) = \sqrt{F_x^{\,2}\big|_{\alpha\neq 0} + F_y^{\,2}\big|_{s_x\neq 0}} \tag{3.16}$$

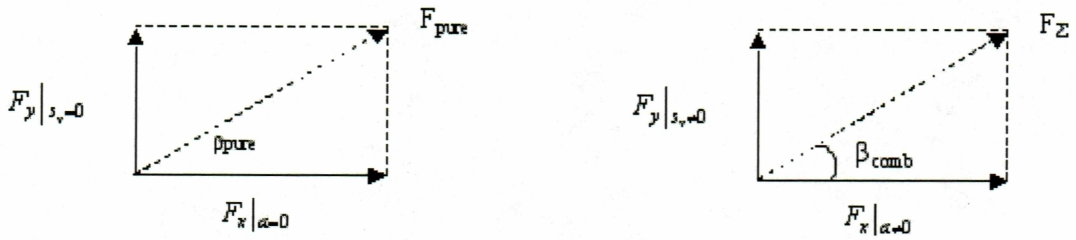

Figure 3.2 Longitudinal and lateral components of pure and combined shear forces

A numerical method is applied to compare the magnitude of F_{pure} (3.13) & F_Σ (3.16). F_{pure} (3.13) is based on the assumption that the shear forces at the tire/terrain interface are linear with respect to normal force. F_Σ (3.16) is based on the non-linearity of the shear forces at the tire terrain interaction, which is proven experimentally. It is easy to obtain F_{pure} as there are published data of pure longitudinal and pure lateral shear forces. But it is comparatively difficult to obtain data of combined lateral force and combined longitudinal force F_Σ. Therefore, the comparison between F_{pure} and F_Σ was not based

on experimental data, but was based on computational results obtained using equations (3.13) and (3.16).

To do the comparison of the pure and combined forces we first need to find appropriate ways to calculate the magnitude of the parameters used in the shear force calculation. The parameters are tire stiffness, friction coefficient, and the constants in the shear distribution equation (3.10). In this study, the parameters are assumed to be functions of normal load F_z. The coefficients of parameter function are derived by curve fitting using the FEA data. In the next section we will discuss how to identify the appropriate values of the coefficients used in each parameter function.

3.2 Coefficient Identification for Tire Stiffness and Friction Coefficient Equations

FEA [42] has been applied to simulate the performance of a tire on fresh snow. The simulations are carried out for loads varying from 3.5 KN to 7.5 KN on a tire of 0.736 m diameter. Thus obtained FEA data are used to find the coefficients in the equations for the tire stiffness, friction coefficient and contact pressure constant are shown in Table 3.2.

Table 3.2 FEA data for the tire stiffness, friction coefficient and pressure constant

Normal Load Fz	Long. Stiffness (KN/radian)C_s	Lateral. Stiffness (KN/radian)C_α	Long.Friction Coefficient μ_x	Lateral.Friction Coefficient μ_y	Pressure Constant E_1
3.5	4.9236	5.85986746	0.39290586	0.22346521	0.04024988
4.5	4.9778	6.10045272	0.35743519	0.18417462	0.08024988
6.24	5.0888	6.34103797	0.29058663	0.13833560	0.18907413
7.5	5.9020	7.17498769	0.24965893	0.11632469	0.34697080

The empirical equations used for the calculations of the longitudinal stiffness and the lateral stiffness are given in equations (3.17, 3.18). The appropriate values of A_4, and A_5 are obtained by optimization, using FEA data given in Table 3.2

$$C_S = \frac{F_Z}{A_4 + A_5 F_Z} \tag{3.17}$$

Where

C_S -longitudinal tire stiffness (KN/rad)

F_Z -normal Load (KN)

A_4 =0.2026 A_5 =0.1516$(KN)^{-1}$

Similarly the values of B_4, and B_5 for lateral stiffness are obtained.

$$C_\alpha = \frac{F_Z}{B_4 + B_5 F_Z} \tag{3.18}$$

Where

C_α -lateral tire stiffness (KN/rad)

$B_4 = 0.1936$ $B_5 = 0.1190(KN)^{-1}$

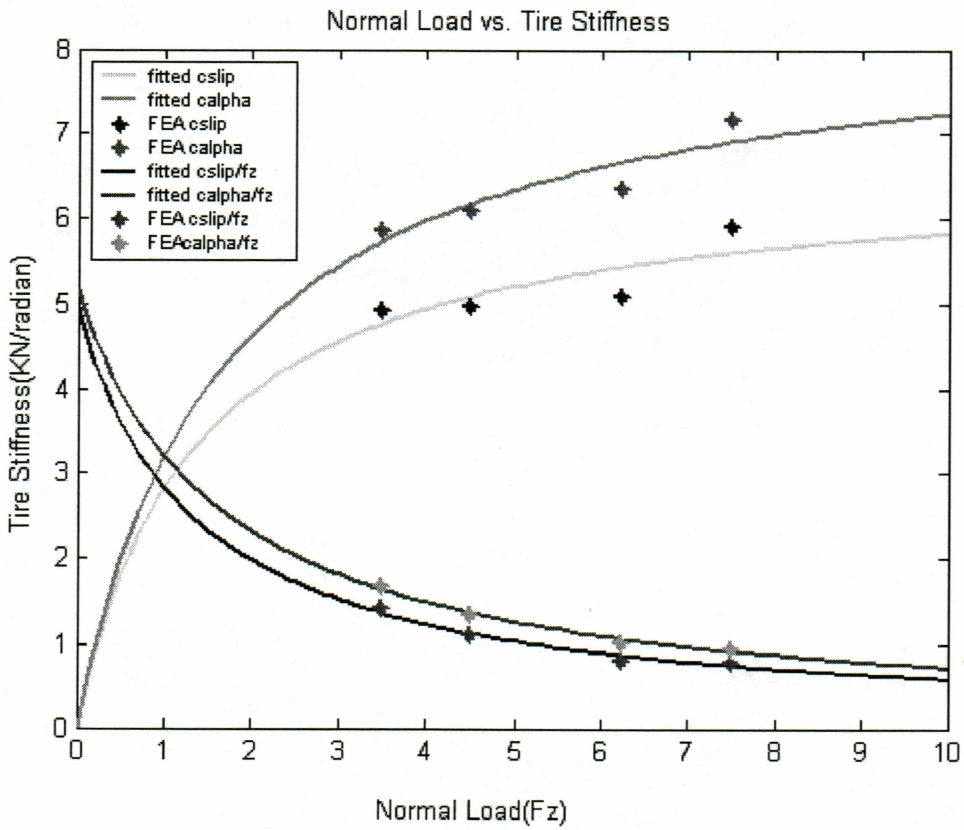

Figure 3.3 Comparison of the fitted curve and FEA data for C_S and C_α

The empirical equations (3.19, 3.20) are used for the calculations of the longitudinal and the lateral friction coefficients, where the constants A_1, A_2, A_3 are also obtained by an optimization method, using the FEA data given in Table 3.2.

$$\mu_X = A_1 + A_2 F_Z + A_3 F_Z^{\,2} \tag{3.19}$$

Where

μ_X -longitudinal friction coefficient

$A_1 = 0.5386 \quad A_2 = -0.0438\,(KN)^{-1} \quad A_3 = 6.9010\text{e-}004\ (KN)^{-2}$

Similarly the values of A_1, A_2, A_3 for lateral stiffness are obtained.

$$\mu_y = B_1 + B_2 F_Z + B_3 F_Z^{\,2} \tag{3.20}$$

μ_y -Lateral Friction Coefficient

$B_1 = 0.4131 \quad B_2 = -0.0673\ (KN)^{-1} \quad B_3 = 0.0037\,(KN)^{-2}$

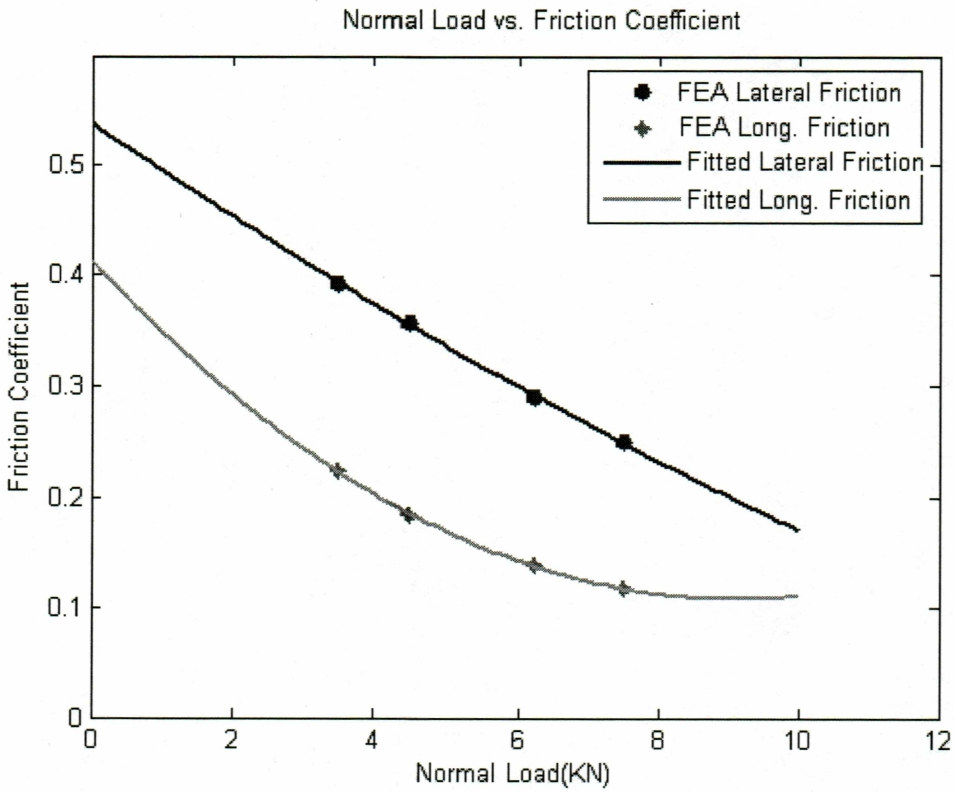

Figure 3.4 Comparison of the FEA data and fitted curve for the friction coefficient

The empirical equation (3.21) is used for the calculation of the contact pressure constant as shown in equation (3.10), where the constants a_1, a_2, are obtained by optimization, using the FEA data given in Table 3.2.

$$E1 = 0.5\left\{1 - \exp\left(-a_1^{\,2} F_z - a_2^{\,2} F_z^{\,2}\right)\right\} \tag{3.21}$$

a_1=7.5852e-009 a_2=0.1203

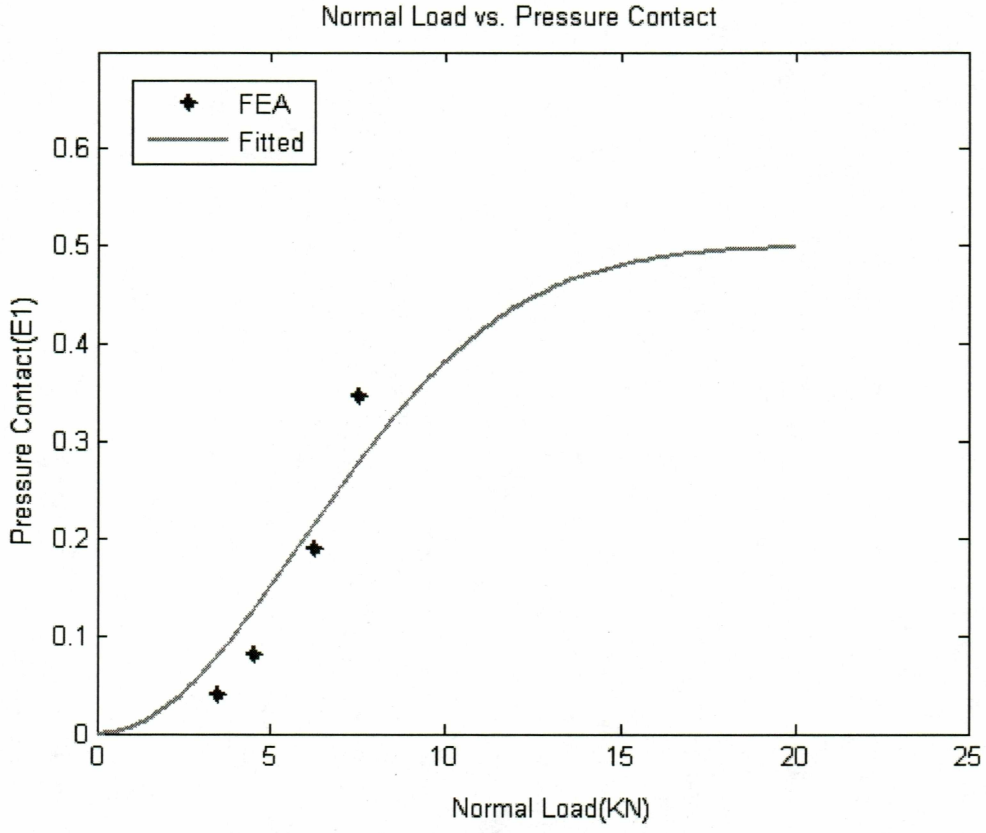

Figure 3.5 Comparison of the FEA data and fitted curve for the contact pressure constant

3.3 Sensitivity Analysis

Now let us study the effect of change in each parameter on the shear force.

3.3.1 Sensitivity due to Percentage Change in Parameters (pure longitudinal slip)

In this section we will study the sensitivity of shear force to each parameter. To study this we changed one parameter and kept the other parameters constant. For instance if we change tire stiffness, the other two parameters, friction coefficient and contact pressure constant, are kept constant. A similar procedure is followed for the other two parameters, as shown in Figure 3.6. Therefore we know the effect of each parameter on shear force. We did the analysis by considering equation (3.11) and studying the effect of a change in each parameter on shear force, defined as shown below

Shear force variation ratio due to c_s $= \dfrac{F_x(F_{z2},\mu_{x1},c_{s2},E_{11}) - F_x(F_{z1},\mu_{x1},c_{s1},E_{11})}{F_x(F_{z2},\mu_{x2},c_{s2},E_{12}) - F_x(F_{z1},\mu_{x1},c_{s1},E_{11})}$

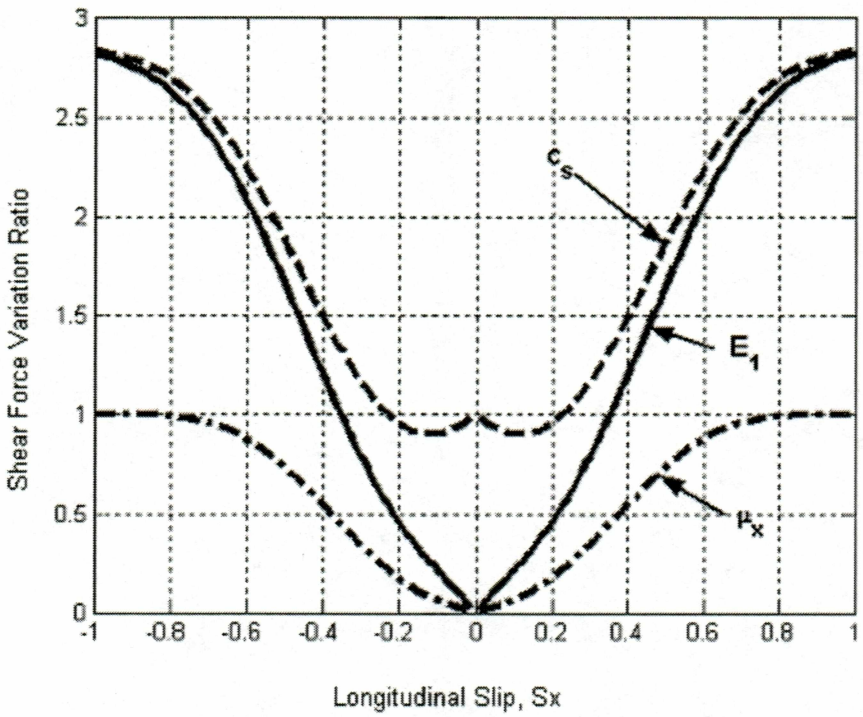

Figure 3.6 Comparison of the shear force variation due to change of each parameter

Shear force variation ratio due to μ_x $= \dfrac{F_x(F_{z2},\mu_{x2},c_{s1},E_{11}) - F_x(F_{z1},\mu_{x1},c_{s1},E_{11})}{F_x(F_{z2},\mu_{x2},c_{s2},E_{12}) - F_x(F_{z1},\mu_{x1},c_{s1},E_{11})}$

Shear force variation ratio due to $E_1 = \dfrac{F_x(F_{z2},\mu_{x1},c_{s1},E_{12}) - F_x(F_{z1},\mu_{x1},c_{s1},E_{11})}{F_x(F_{z2},\mu_{x2},c_{s2},E_{12}) - F_x(F_{z1},\mu_{x1},c_{s1},E_{11})}$

We can infer from Figure 3.6 that the shear force variation ratio is always positive, which means that, as the normal force increases, the shear force also increases. The tire stiffness has the greatest influence and the coefficient of friction has the least influence among all the parameters on the shear force variation ratio, when we take magnitude into consideration.

The contact pressure constant (E_1) has a greater influence on the shear force variation ratio when we consider slope, until partial slip (S_x<0.8). At the full slip the shear force is sensitive to neither the stiffness nor the contact pressure.

In the next section we compare the effect of each parameter on shear force variation under different conditions (i.e., by considering different tires with differing stiffness, and also various terrains having differing friction coefficients).

3.3.2 Sensitivity due to Change of Tire Stiffness (pure longitudinal slip)

The change physically indicates that we are considering different tires, having different stiffness. Let us change tire stiffness as shown in Figure 3.7. The arbitrary values of tire stiffness should be chosen in such a way that they should satisfy the basic increasing trend of $C_s\ Vs\ F_z$ and decreasing trend of $C_s / F_z\ Vs\ F_z$ as shown in Figure 3.9. We can also observe that the slopes of each curve follow relation $OA < OB < OC$ for $C_s\ Vs\ F_z$ and $OA > OB > OC$ for $C_s / F_z\ Vs\ F_z$.

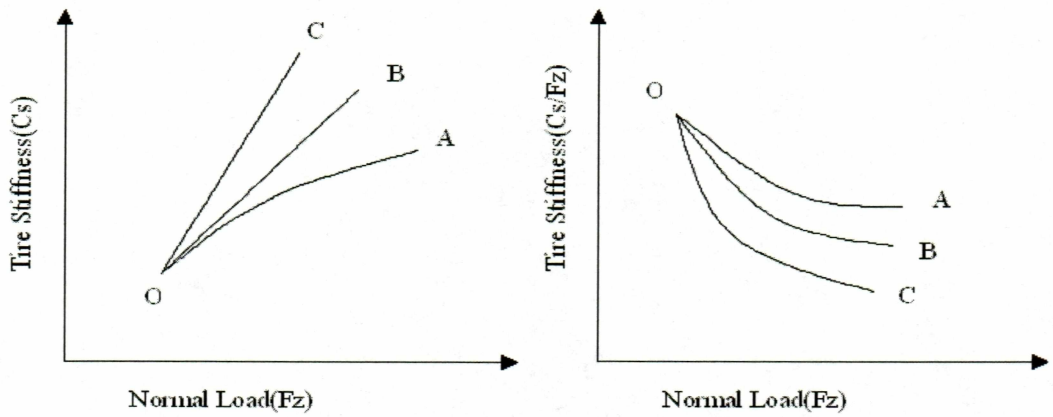

Figure 3.7. Trend change of tire stiffness

Figure 3.8 uses equation (3.11) to show the shear force variation due to the change of the stiffness as shown in Figure 3.7. Shear force variation for curve A in Figure 3.8 is defined as $F_x(F_{z2},\mu_{x2},c_{s2},E_{12})-F_x(F_{z1},\mu_{x1},c_{s1},E_{11})$. Shear force variation for curve B in Figure 3.8 is defined as $F_x(F_{z1},\mu_{x1},c_{s1},E_{11})-12(random1)$. Shear force variation for curve C in Figure 3.8 is defined as $F_x(F_{z1},\mu_{x1},c_{s1},E_{11})-18(random2)$.

As we design the trend of each curve according to Figure 3.9, the shear force variation increases for a small slip, up to 0.2. For the slip between 0.2 and 0.5 the shear force variation decreases. At the full slip condition, irrespective of the change in the tire stiffness, the shear force variation remains constant.

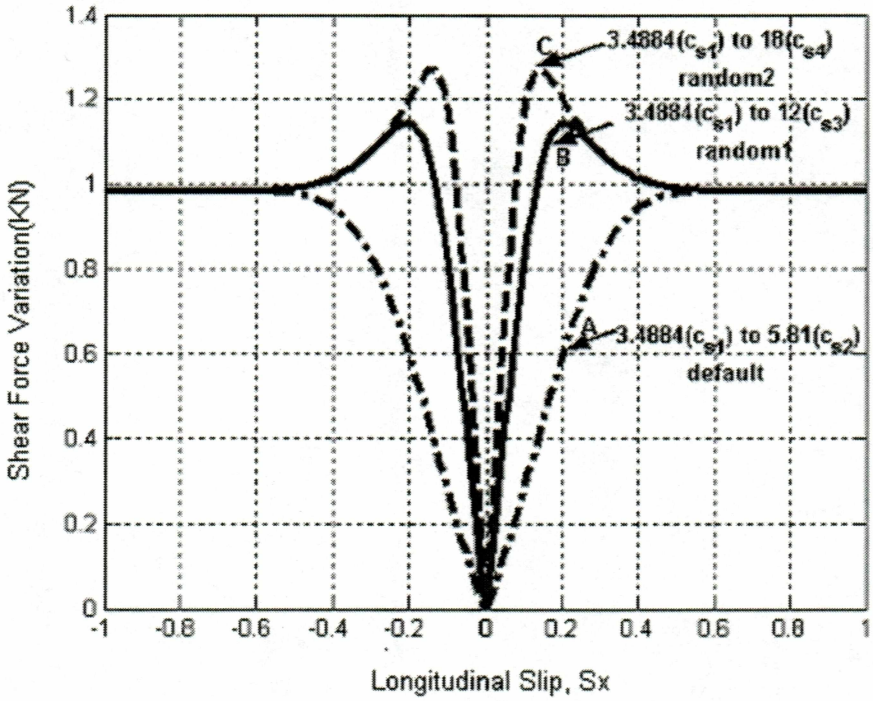

Figure 3.8 Comparison of the shear force at different ranges of stiffness

3.3.3 Sensitivity due to Change of Contact Pressure Constant

Let us change the trend of pressure constant vs. normal load, as shown in Figure 3.9. The arbitrary values of contact pressure constant should be chosen in such a way that they

should satisfy the basic increasing trend of $E_1 \, Vs \, F_z$ as shown in Figure 3.9. From Figure 3.9 we can also observe that the slope of each curve follows the relation $OA < OB < OC$ for $E_1 \, Vs \, F_z$.

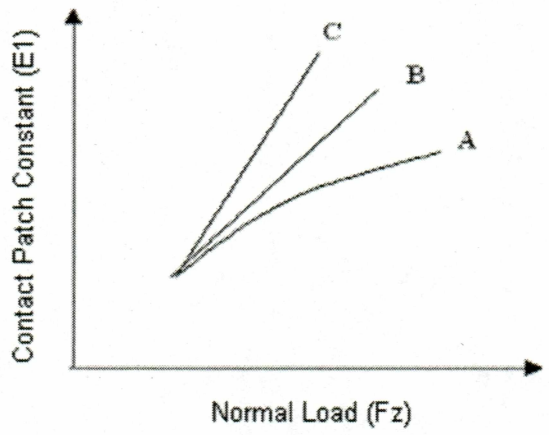

Figure 3.9 Trend of contact patch constant

As we design the trend of each curve according to the Figure 3.9, the slope of relative shear force increases as the slope of the curves increases up to partial slip i.e., 0.6. At the full slip condition, irrespective of the trend change in the contact pressure constant, the relative shear force for all the curves (OA, OB, OC) remains the same, as shown in Figure 3.12

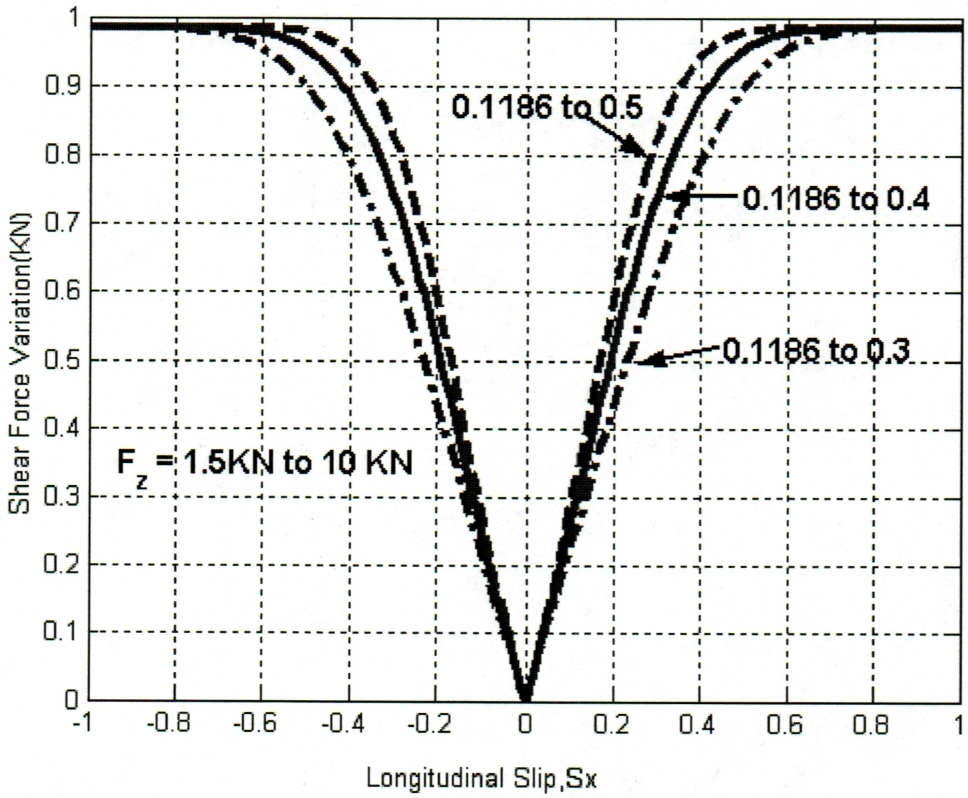

Figure 3.10 Comparison of the shear force variation due to change in contact patch constant

3.3.4 Sensitivity due to Change of Friction Coefficient

Let us change the trend of the friction coefficient, μ_x and the normal load F_z as shown in Figure 3.11. The arbitrary values of friction coefficient should be chosen in such a way that they satisfy the basic decreasing trend of $\mu_x Vs\ F_z$ and increasing trend of $\mu_x F_z\ Vs\ F_z$. The curve 'b', which we obtained with the initial point 0.3938 and final point 0.1696, is from the equation $\mu_x = a_1 + a_2 F_z + a_3 F_z^2$, where the values of a_1, a_2, a_3 are obtained from the optimization using the FEA data.

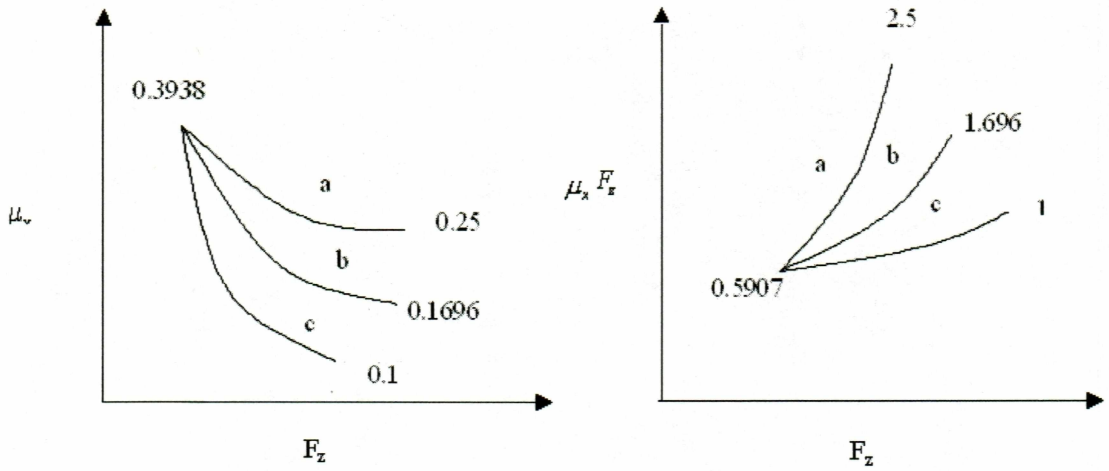

Figure 3.11 Trend of friction coefficient

Now if we design the values of μ_x so that we get two curves, 'c' and 'a' which are below and above the curve 'b' as shown in Figure 3.11, we can observe that for the curve 'c' the relative shear force is unstable at very small slips, up to 0.25, and then it increases as shown in Figure 3.12. This situation occurs when the vehicle moves from fresh snow with high friction to slippery ice with low friction. At full slip the relative shear force remains constant.

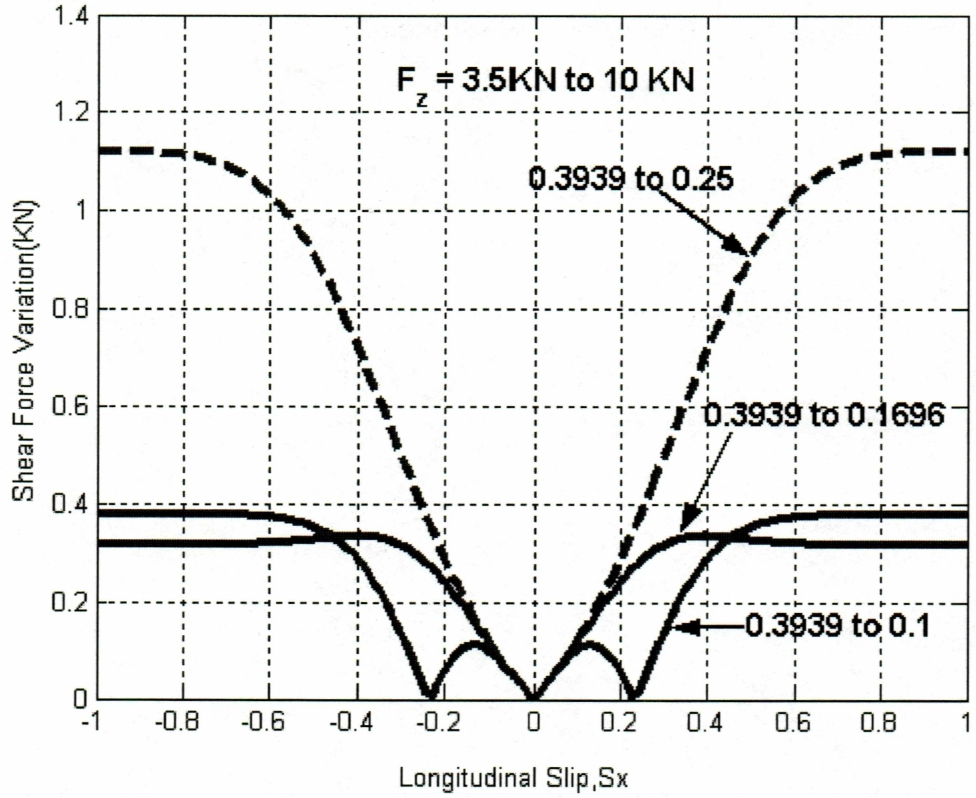

Figure 3.12 Comparison of the shear force variation due to change in friction coefficient

3.4 Numerical Comparison of Pure and Combined Forces

3.4.1 Comparison of F_{pure} and $F_{combined}$ Magnitude

From Figure 3.13 we can observe that F_{pure} (equation (3.13)) is always greater than the $F_{combined}$ (3.16). At constant normal load and as the slip angle increases, F_{pure} increases whereas $F_{combined}$ decreases. At a constant slip angle, as the normal load changes F_{pure} and $F_{combined}$ increase.

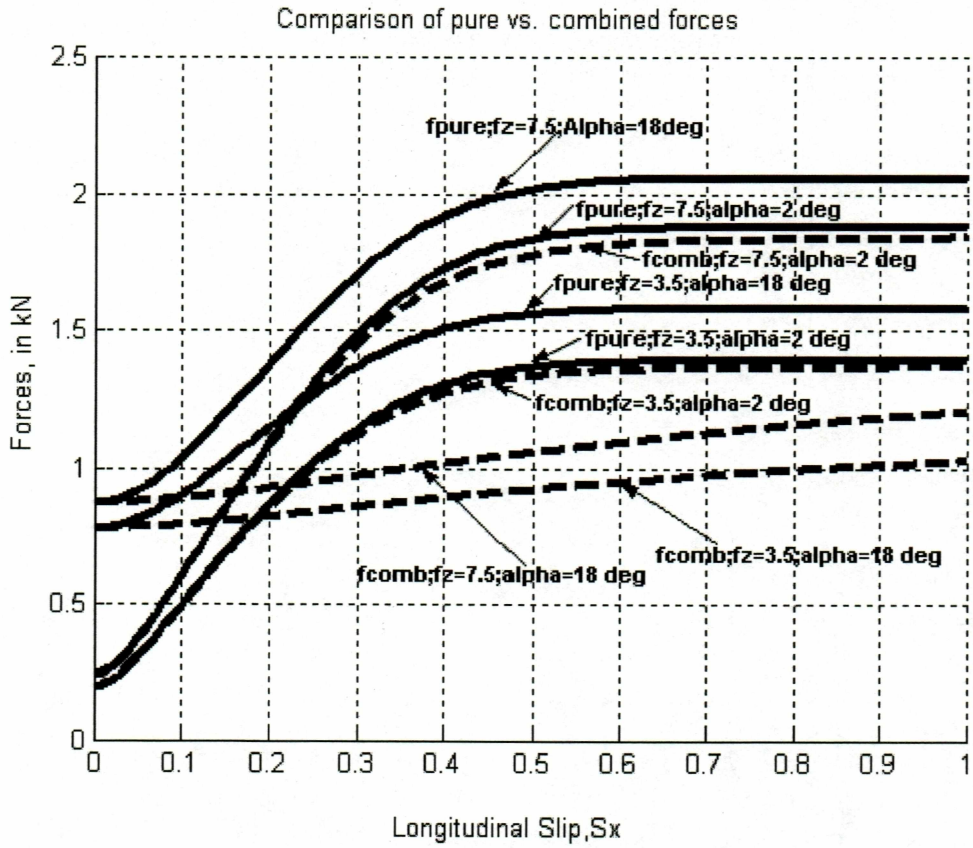

Figure 3.13 Comparison of magnitude the pure and combined forces

3.4.2 Comparison of Angle β F_{pure} and $F_{combined}$

We compared angle β for both pure and combined forces as shown in Figure 3.2. We can observe that at smaller slips the pure and the combined forces are closer to 90^0, which indicates that the lateral force is dominating more. At the intermediate slips both the combined and the pure force curves are close to 45^0, since the lateral and the longitudinal forces have almost equal influence. At the full slip condition both the pure and the combined force angles are close to zero, since the longitudinal force dominates. We can also observe that the normal load does not have any influence on the pure and the combined force orientation.

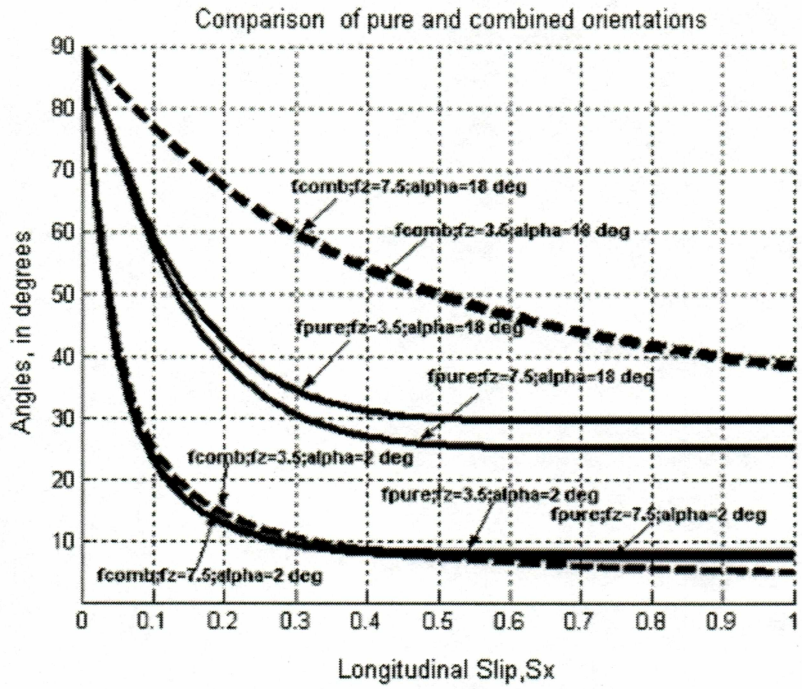

Figure 3.14 Comparison of the orientation of pure and the combined forces

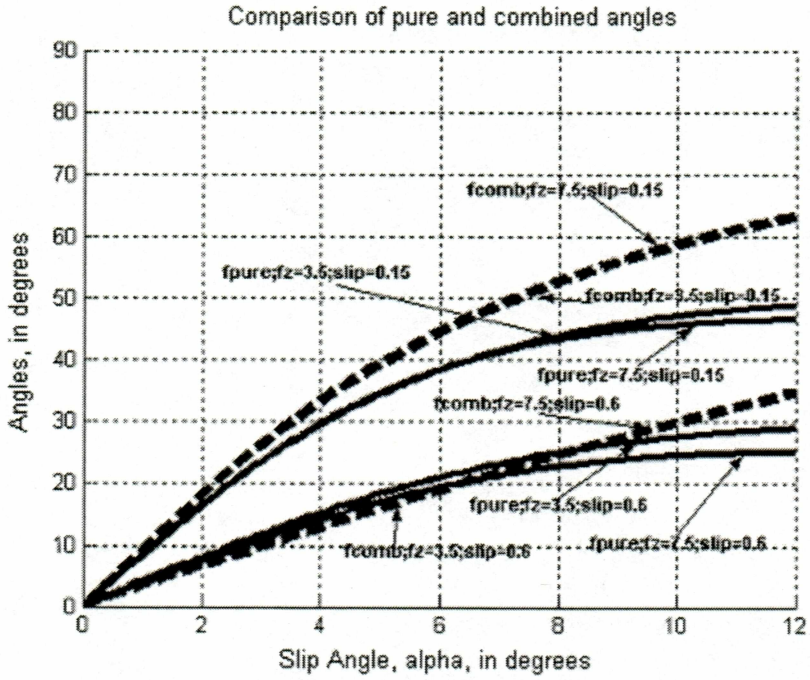

Figure 3.15 Comparison of the orientation of pure and combined forces w.r.t. slip angle

3.4.3 Comparison of Isotropic and Anisotropic Cases

Figure 3.16 shows the comparison of pure and combined shear forces for the isotropic case(equal friction coefficient in all directions, $\mu_x = \mu_y$) and the anisotropic cases (unequal friction coefficients, $\mu_x \neq \mu_y$). For both the isotropic and anisotropic cases the β_{comb} is independent of the coefficient of friction and the normal load as shown in Figure 3.18.

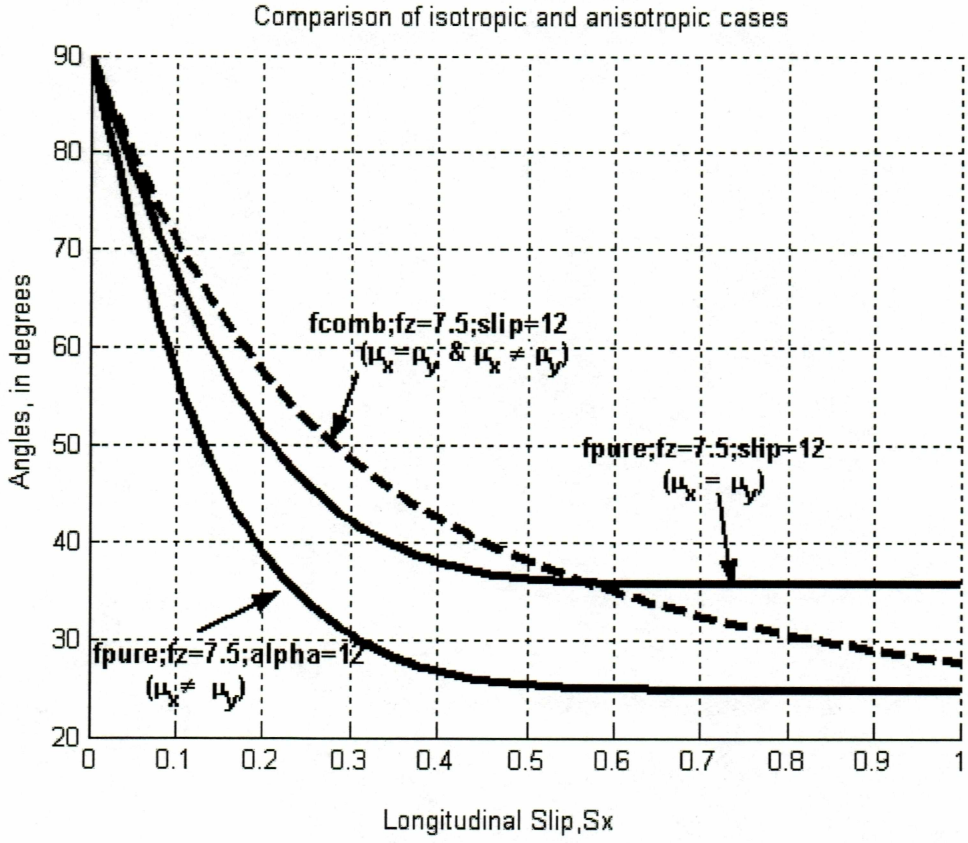

Figure 3.16 Comparison of the pure and combined forces for isotropic and anisotropic cases.

3.5 Summary

In this chapter we expressed shear force as a function of normal load, slip, slip angle and other snow/tire property-related parameters. Material property parameters include tire stiffness, friction coefficient and contact pressure constant. In order to simplify the shear force model, material property parameters are assumed to be functions of normal load only. We obtain the coefficients of empirical equations through curve fitting using FEA data. FEA data include simulated values of tire stiffness, friction coefficient and contact pressure constant for specific tire/snow pairs under different loads. According to computation results obtained from the parameter empirical equations, the selected parameter functions can appropriately reproduce the FEA data well in both magnitude and trend. We studied the effect of each parameter, i.e., friction coefficient, tire stiffness and contact pressure constant, on the shear force. We found that for different tires having different stiffness the shear force increases as the tire stiffness increases. We also found that for different terrain with different friction coefficients, the shear force increases with an increase in friction coefficient.

We compared the resultant shear force obtained by two methods. In the first method we assumed shear forces obey a linear system, and obtained the resultant shear force by taking the vector sum of pure longitudinal and pure lateral forces. In the second method we assumed shear forces obey a non-linear system, and obtained the resultant shear force by taking the vector sum of combined longitudinal and combined lateral shear force. We found that the resultant shear forces obtained by these two methods are not the same, but the resultant shear force due to pure forces is always greater than the resultant shear force due to combined shear forces. So we use the second method to obtain the resultant shear force, which has more practical importance, as the prediction of shear force matches the experimental data and FEA simulation results better.

4. Semi-Analytical Shear Stress Model For Shallow Snow

The main objective of this chapter is to develop a semi-analytical shear stress model for tire–snow interaction as a function of normal pressure and slip. The existing classic shear stress model has a number of terrain constants, such as cohesion, friction angle, shear modulus, etc., which are difficult to quantify for snow. So we planned to develop a semi-analytical equation with a minimum number of parameters, which has a great advantage of reducing the computational time while conducting the vehicle simulations. To achieve this goal we used numerical method and matched the boundary conditions of shear stress of the existing classic shear displacement model [1, 7, 14] with our model. We compared the computation results of both the models, which matched reasonably well with respect to the boundary values.

By using the above two models we calculated the sinkage and the Motion resistance as a function of slip, and compared with the FEA data which matched reasonably well.

To explain all the computation and comparison processes we first need to describe the parameters used in these processes.

4.1.Wong's Pressure Sinkage Relationship

Wong [4] has conducted many experiments for tire moving on snow layers and found that sinkage can be represented as an exponential function of pressure (i.e. normal stress).

$$z = z_w\left[1-\exp\left(-\frac{c}{p_w}\bar{\sigma}_n\right)\right] = z_w(1-Z) \tag{4.1a}$$

(or)

$$\bar{\sigma}_n = \frac{\sigma_n}{c} = \left(\frac{p_w}{c}\right)\left[-\ln\left(1-\frac{z}{z_w}\right)\right] = \left(\frac{p_w}{c}\right)(-\ln Z) \tag{4.1b}$$

Normalized pressure is given by equation (4.2)

$$\bar{\sigma}_n = \frac{\sigma_n}{c} \tag{4.2}$$

Relative sinkage is given by equation (4.3)

$$Z = 1 - \frac{z}{z_w} = \exp\left(- \frac{c}{p_w} \overline{\sigma}_n \right) \tag{4.3}$$

Relative sinkage at maximum sinkage is

$$Z_0 = 1 - \frac{z_0}{z_w} \tag{4.4}$$

Where

c-cohesion modulus

σ_n -normal pressure

$\overline{\sigma}_n$ - normalized normal pressure

p_w -upper bound pressure

z_w -upper bound sinkage

Now in order to consider the geometry of the pressure-sinkage relationship, let us assume a rigid wheel moving on the shallow snow instead of the pneumatic wheel, as shown in Figure 4.1. We made this assumption because the pneumatic wheel behaves as rigid wheel on the soft terrain and the shallow snow is a soft terrain. Our main goal is to express all the parameters, i.e., sinkage, motion resistance, drawbar pull, and tractive force, as function of contact angle. Let us first define each parameter in Figure 4.1.

θ -contact angle at any arbitrary point of contact region

θ_0 - maximum contact angle

F_z - normal load acting on the wheel

D -wheel diameter

h_s - snow height

z -sinkage at any arbitrary point

z_0 -maximum sinkage

τ_x - shear stress acting due to tire snow interaction

$F_{\tau x}$ - shear force in x-direction

ω - wheel angular velocity

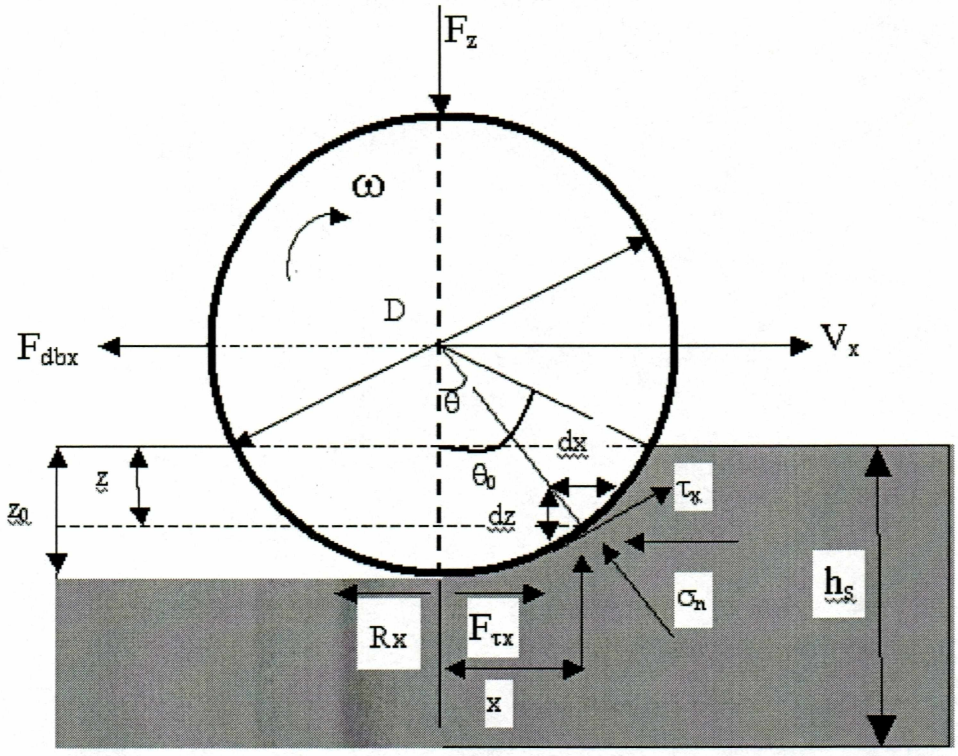

Figure.4.1 Rigid wheel-snow interaction model.

Now let us consider the geometry of each parameter. The sinkage z at any point on the tire-snow interaction can be determined by the equation [47]

$$z = \frac{D}{2}(\cos\theta - \cos\theta_0) \quad \text{(or)} \quad \cos\theta = \frac{2}{D} z + \cos\theta_0 \tag{4.5}$$

From Figure 4.1 the maximum sinkage occurs at $\theta = 0$, and is given by equation (4.6)

$$z_0 = z|_{\theta=0} = \frac{D}{2}(1 - \cos\theta_0) \tag{4.6}$$

From the geometry of Figure 4.1, we also have the relation

$$\left(\frac{D}{2}\sin\theta\right)^2 = (z_0 - z)[D - (z_0 - z)] \tag{4.7}$$

At $\theta = \theta_0$ equation (4.7) takes the form

$$\left(\frac{D}{2}\sin\theta_0\right)^2 = z_0(D - z_0) \tag{4.8}$$

Equations (4.1) to (4.8) describe the relationship between contact pressure and contact angle. There are methods to determine the three-dimensional contact area between a tire and a soil [51].

4.2 Shear Force-Shear Displacement Relationships

We will discuss the two fundamental classic equations in this section. To determine the shear stress as a function of slip and normal pressure, we need to develop an equation for the shear displacement due to tire snow interaction. The shear displacement developed along the contact area of the rigid wheel is determined based on the slip velocity (V_j), as shown in Figure 2.8. For a rigid wheel, the velocity V_j of a point on the rim is the tangential component of the absolute velocity at the point, as shown in Figure 2.8. The magnitude of V_j of a point on the rim defined by the angle θ can be expressed by [4]

$$V_j = r\omega\left[1 - (1 - i)\cos\theta\right] \tag{4.9}$$

Where

r - wheel radius

i - slip of the wheel

The shear displacement, which is the integration of shear velocity along the wheel snow interaction, is given by [4]

$$j_x = \frac{D}{2}\left[(\theta_0 - \theta) - (1 - i)(\sin\theta_0 - \sin\theta)\right] \tag{4.10}$$

Where

θ_0 - maximum contact angle

The shear stress acting at the interface is given by [4]

$$\tau_x = (c + \sigma_n \tan\phi)[1 - \exp(-j_x / K_{\text{shear}})] \tag{4.11}$$

Where

c- cohesion modulus

σ_n -normal pressure

ϕ -friction angle

K_{shear} -shear modulus

j_x -shear displacement

From the above equations it is clear that we need many snow parameters (i.e. c, ϕ, K_{shear}) to calculate the shear stress at the tire-snow interaction. To obtain these parameters we would need to conduct many experiments [52], such as plate sinkage tests to calculate the normal pressure and shear tests to calculate the shear modulus, cohesion and internal friction angle of the terrain while this is a robust procedure, it is impractical. In order to eradicate this problem we planned to develop a semi-analytical equation for shear stress, which is a function of normal pressure (σ_n) and slip (i) only. We implemented a numerical approach to achieve this goal.

We introduced five dimensionless input parameters, of which two are geometric constants and the three are material constants.

Geometric constants: $\frac{z_w}{D}, \theta_0$

Material constants: $\frac{c}{p_w}, u_k, \tan\phi$

Where

z_w -upper bound sinkage[53]

$$u_k = \frac{D}{K_{shear}}$$

p_w-upper bound pressure [53]

The input values we assumed to numerically find the boundary conditions are shown in Table 4.1

Table 4.1 The geometric constants and material constant values

Geometric constants	$\frac{z_w}{D}$=0.2717	θ_0=53.6747(deg)=0.9398(rad)	
Material constants	$\frac{c}{p_w}$=0.2165	$u_k = \frac{D}{K_{shear}}$=73.6	$\tan\phi$= 0.0787

We needed the boundary conditions of the existing equation to set the new empirical equation. For this we found the first order and the second order derivatives of the existing equation. By doing this we came to the following conclusion.

Let $y = f(x)$ be a function

$\frac{dy}{dx} > 0$ indicates the function $f(x)$ is monotonic and increasing

$\frac{dy}{dx} < 0$ indicates the function $f(x)$ is monotonic and decreasing

$\frac{dy}{dx} > 0$ and $\frac{d^2y}{dx^2} > 0$ indicates the function $f(x)$ increases rapidly and possibly tends to infinity

$\frac{dy}{dx} > 0$ and $\frac{d^2y}{dx^2} < 0$ indicates the function $f(x)$ increases slowly and possibly tends to a constant limit

As we want to get shear stress as a function of normal pressure (σ_n) and slip (i), we calculated the first order and the second order derivatives of shear force with respect

to normal pressure (σ_n) and slip (i). The boundary conditions of each parameter used in the equation derivation are shown in the Table [4.2]

Table 4.2 Boundary conditions of each parameter of equation (4.12)

	θ	z	Z	$\bar{\sigma}_n$	J	J_k
zero sinkage	θ_0	0	1	0	0	u_k
max. sinkage	0	z_0	$Z_0 = 1 - \frac{z_0}{z_w}$	$\bar{\sigma}_{n0} = \left(\frac{p_w}{c}\right)(-\ln Z_0)$	$J_0 = \frac{1}{2}(\theta_0 - \sin\theta_0) + \frac{i}{2}\sin\theta_0$	$J_{k0} = u_k \exp(-u_k J_0)$

Equation (4.12) is the fundamental non-dimensional shear stress equation, which we used for our derivations.

$$\bar{\tau}_x = \left(1 + \bar{\sigma}_n \tan\phi\right)\left(1 - \frac{J_k}{u_k}\right) \tag{4.12}$$

Where

$$\bar{\tau}_x = \frac{\tau_x}{c}$$

$$\bar{\sigma}_n = \frac{\sigma_n}{c}$$

$$J_k = u_k \exp(-u_k J)$$

$$u_k = \frac{D}{K_{shear}}$$

The final derived equations are tabulated in Table 4.3, and the derivations are shown in the appendix in detail.

Table 4.3 The first and second order derivatives of equation (4.12)

	First order	Second order
$\bar{\tau}_x$ vs. $\bar{\sigma}_n$	$y_1 = \frac{\partial \bar{\tau}_x}{\partial \bar{\sigma}_n}$ $= \tan\phi\left(1-\frac{J_k}{u_k}\right)+T_0\left(T_1+T_2\right)\geq 0$	$y_2 = \frac{\partial^2 \bar{\tau}_x}{\partial \bar{\sigma}_n^2} = -T_0^2\left(T_1 T_3 + T_2 T_4\right)+T_0 T_\Delta$ $\approx -T_0^2\left(T_1 T_3 + T_2 T_4\right) \approx -T_0^2\left(T_1+T_2\right)^2 \leq 0$
$\bar{\tau}_x$ vs. i	$y_3 = \frac{\partial \bar{\tau}_x}{\partial i}$ $= \frac{1}{2} J_k\left(1+\bar{\sigma}_n \tan\phi\right)\left(\sin\theta_0 - \sin\theta\right)\geq 0$	$y_4 = \frac{\partial^2 \bar{\tau}_x}{\partial i^2} = -\frac{1}{2} u_k\left(\sin\theta_0 - \sin\theta\right) y_3 \leq 0$

Where:

$$J = \frac{1}{2}\left[\left(\theta_0 - \theta\right) - \left(1-i\right)\left(\sin\theta_0 - \sin\theta\right)\right]$$

$$Z = 1 - \frac{1}{2}\left(\frac{D}{z_w}\right)\left(\cos\theta - \cos\theta_0\right)$$

$$J_k = u_k \exp\left(-u_k J\right)$$

$$\bar{\sigma}_n = \left(\frac{p_w}{c}\right)\left(-\ln Z\right)$$

$$T_0 = Z\left(\frac{z_w}{D}\right)\left(\frac{c}{p_w}\right)$$

$$T_\Delta = \left[\left(2J_k \tan\phi\right) - \left(\frac{c}{p_w}\right) J_k\left(1+\bar{\sigma}_n \tan\phi\right)\right]\left[\left(i\frac{\cos\theta}{\sin\theta}\right)+\left(\frac{1-\cos\theta}{\sin\theta}\right)\right]$$

$$T_1 = J_k\left(1+\bar{\sigma}_n \tan\phi\right)\left(i\frac{\cos\theta}{\sin\theta}\right)$$

$$T_2 = J_k\left(1+\bar{\sigma}_n \tan\phi\right)\left(\frac{1-\cos\theta}{\sin\theta}\right)$$

$$T_3 = -\frac{2}{\sin^2\theta}\left(\frac{1}{\cos\theta}\right)+u_k\left(i\,\frac{\cos\theta}{\sin\theta}\right)+2u_k\left(\frac{1-\cos\theta}{\sin\theta}\right)$$

$$T_4 = \frac{2}{\sin^2\theta}+u_k\left(\frac{1-\cos\theta}{\sin\theta}\right)$$

From Table 4.2 it is clear that the first order derivative $\frac{\partial \bar{\tau}_x}{\partial \bar{\sigma}_n} \geq 0$ $\frac{\partial^2 \bar{\tau}_x}{\partial \bar{\sigma}_n^2} \leq 0$ indicates that the $\bar{\tau}_x$ *vs* $\bar{\sigma}_n$ curve is increasing slowly and possibly tends to a constant limit as shown in Figures 4.2 and 4.3 In the same way $\frac{\partial \bar{\tau}_x}{\partial i} \geq 0$ and $\frac{\partial^2 \bar{\tau}_x}{\partial i^2} \leq 0$, which indicates that the $\bar{\tau}_x$ *vs* $\bar{\sigma}_n$ curve is increasing slowly and possibly tends to a constant limit, as shown in Figures 4.4 and 4.5. We then numerically found the boundary values, at the maximum sinkage and zero sinkage, for all the curves as shown in Table 4.4

Table 4.4 Boundary values at the maximum sinkage and zero sinkage for equation (4.12)

	$\bar{\sigma}_n = 0$ (zero sinkage)	$\bar{\sigma}_n = \bar{\sigma}_{n0}$ (maximum sinkage)	trend
T_0 vs. $\bar{\sigma}_n$	$T_0\big\|_{Z=1} = \left(\frac{z_w}{D}\right)\left(\frac{c}{p_w}\right)$	$T_0\big\|_{Z=Z_0} = Z_0\left(\frac{z_w}{D}\right)\left(\frac{c}{p_w}\right)$	monotonic decreasing
$T_1 + T_2$ vs. $\bar{\sigma}_n$	$u_k(Q_1+Q_2)\big\|_{\theta=\theta_0}$	0	monotonic decreasing
y_1 vs. $\bar{\sigma}_n$	$\left(T_0\big\|_{Z=1}\right)u_k(Q_1+Q_2)\big\|_{\theta=\theta_0}$	$\tan\phi$	monotonic decreasing
y_2 vs. $\bar{\sigma}_n$	- $\left(T_0\big\|_{Z=1}\right)^2 u_k^2\,(Q_1+Q_2)^2\big\|_{\theta=\theta_0}$	0	monotonic decreasing
y_3 vs. $\bar{\sigma}_n$	0	$y_3\big\|_{\theta=0} = \frac{1}{2}\left(J_k\big\|_{\theta=0}\right)\left(1+\bar{\sigma}_{n0}\tan\phi\right)\sin\theta_0$	
y_4 vs. $\bar{\sigma}_n$	0	$-\frac{1}{2}u_k\sin\theta_0\left(y_3\big\|_{\theta=0}\right)$	

4.3 Simplified Shear Model

Depending on the trend and order of magnitude of the existing model described in the previous section, we have developed a simplified semi-empirical equation, which is a function of normal pressure ($\bar{\sigma}_n$) and slip (i) as shown in equation (4.13)

$$\bar{\tau}_x = \left(1+\bar{\sigma}_n\ \tan\phi\right)\left[1-\exp\left(-U_0\right)\right] \tag{4.13}$$

Where

$$U_0 = \left(i+\tau_2\right)\tau_1\,\bar{\sigma}_n + \frac{1}{6}\left(2i-i^2\right)\tau_1\,\bar{\sigma}_n^3$$

$$\tau_1 = u_k\left(\frac{z_w}{D}\right)\left(\frac{c}{p_w}\right)\left(\frac{\cos\theta_0}{\sin\theta_0}\right) > 0$$

$$\tau_2 = \left(\frac{1}{\cos\theta_0}\right) - 1 > 0$$

Table 4.5 The first order and the second order derivatives of equation (4.13).

	First order	Second order
$\bar{\tau}_x$ vs. $\bar{\sigma}_n$	$y_1 = \frac{\partial \bar{\tau}_x}{\partial \bar{\sigma}_n} = \tan\phi + [U_1(1+\bar{\sigma}_n \tan\phi) - \tan\phi]\exp(-U_0)$	$y_2 = \frac{\partial^2 \bar{\tau}_x}{\partial \bar{\sigma}_n^2} = 2(U_1 \tan\phi)\exp(-U_0) - (U_1^2 - U_2)(1+\bar{\sigma}_n \tan\phi)\exp(-U_0)$
$\bar{\tau}_x$ vs. i	$y_3 = \frac{\partial \bar{\tau}_x}{\partial i} = (1+\bar{\sigma}_n \tan\phi) U_3 \exp(-U_0)$	$y_4 = \frac{\partial^2 \bar{\tau}_x}{\partial i^2} = -\left(U_3 - \frac{U_4}{U_3}\right) y_3$

Where:

$$U_1 = \tau_1(i+\tau_2) + \left(\frac{1}{2}\bar{\sigma}_n\right) U_2$$

$$U_2 = (2i - i^2)(\tau_1 \bar{\sigma}_n)$$

$$U_3 = (\tau_1 \bar{\sigma}_n) - (1-i)\, U_4$$

$$U_4 = -\frac{1}{3}\left(\tau_1 \bar{\sigma}_n^3\right)$$

We then numerically calculated the boundary conditions, at the zero sinkage and the maximum sinkage of the new model, and tabulated the results in the Table 4.5. The inputs of the existing shear displacement model are shear displacement, contact angle, normal pressure and slip. The simplified model takes only normal pressure and slip as the inputs. Thus in the simplified model we have reduced the number of inputs, when compared to the existing shear displacement model.

Table 4.6 shows the boundary conditions at the zero and maximum sinkage of equation (4.13)

Table 4.6 Boundary conditions at the zero and maximum sinkage of equation (4.13)

	$\bar{\sigma}_n = 0$ (zero sinkage)	$\bar{\sigma}_n = \bar{\sigma}_{n0}$ (maximum sinkage)	trend
y_1 vs. $\bar{\sigma}_n$	$U_1\|_{\bar{\sigma}_n=0} = \tau_1(i+\tau_2)$	$\tan\phi$	Monotonic decreasing
y_2 vs. $\bar{\sigma}_n$	$-\left(U_1\|_{\bar{\sigma}_n=0}\right)^2 + 2\left(U_1\|_{\bar{\sigma}_n=0}\right)\tan\phi$	0	Monotonic decreasing
y_3 vs. $\bar{\sigma}_n$	0	0	N/A
y_4 vs. $\bar{\sigma}_n$	0	0	N/A

We compare the existing model and the new model numerically, with respect to the order of magnitude and the trend of boundary conditions, which matched very well as shown in Figures 4.2, 4.3, 4.4, 4.5.

From Figure 4.2 we can conclude that the models match well with respect to the following points:

- y_1 *vs* $\bar{\sigma}_n$ is always in the positive region.
- As the normal pressure increases from 0 to 1, y_1 decreases from a maximum value to a certain value.
- As normal pressure increases, y_1 remains constant at approximately $\tan\phi$
- As the slip increases the initial slope increases for both models, and after reaching a certain value of slip they remain constant, irrespective of the change in the slip.

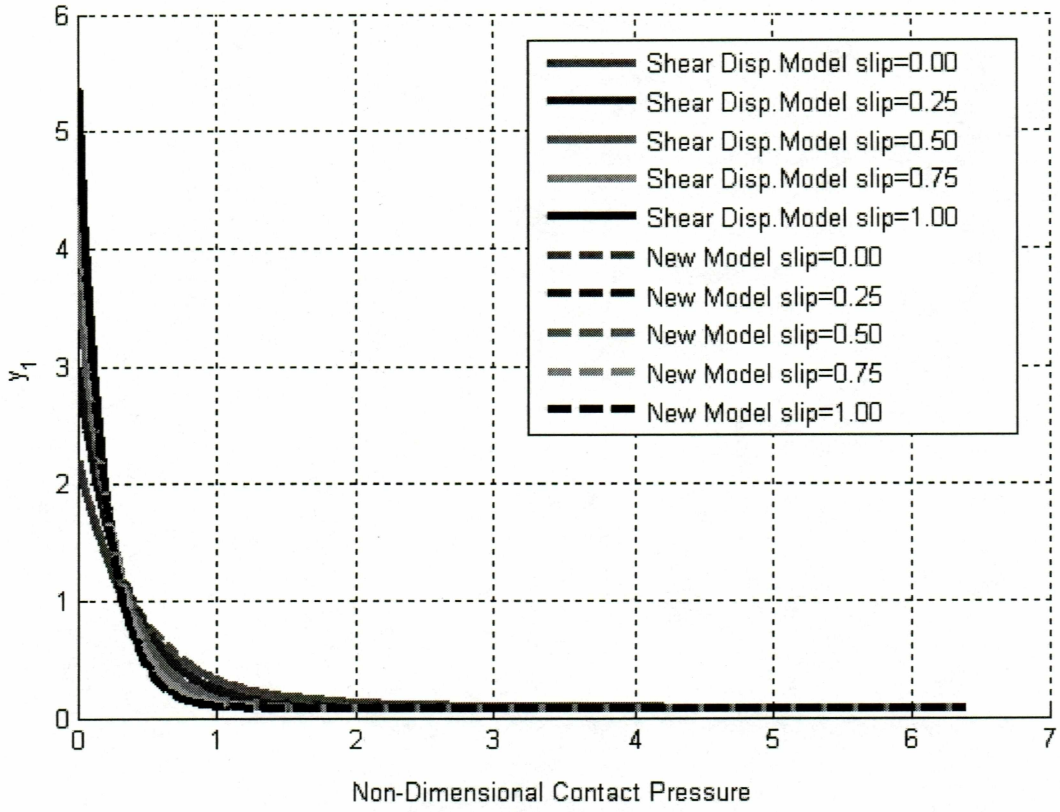

Figure 4.2 Comparison of the first order derivative of both models at various slips

From the Figure 4.3 we can conclude that the models match well with respect to the following points:

- y_2 *vs* $\overline{\sigma}_n$ is always in the negative region.
- As the normal pressure increases from 0 to 1, y_2 decreases from a maximum value to a certain value.
- For values greater than 1, as the normal pressure increases y_2 is always zero.
- As the slip increases the initial slope increases for both models, and then after reaching a certain value of slip they remain zero, irrespective of the change in the slip.

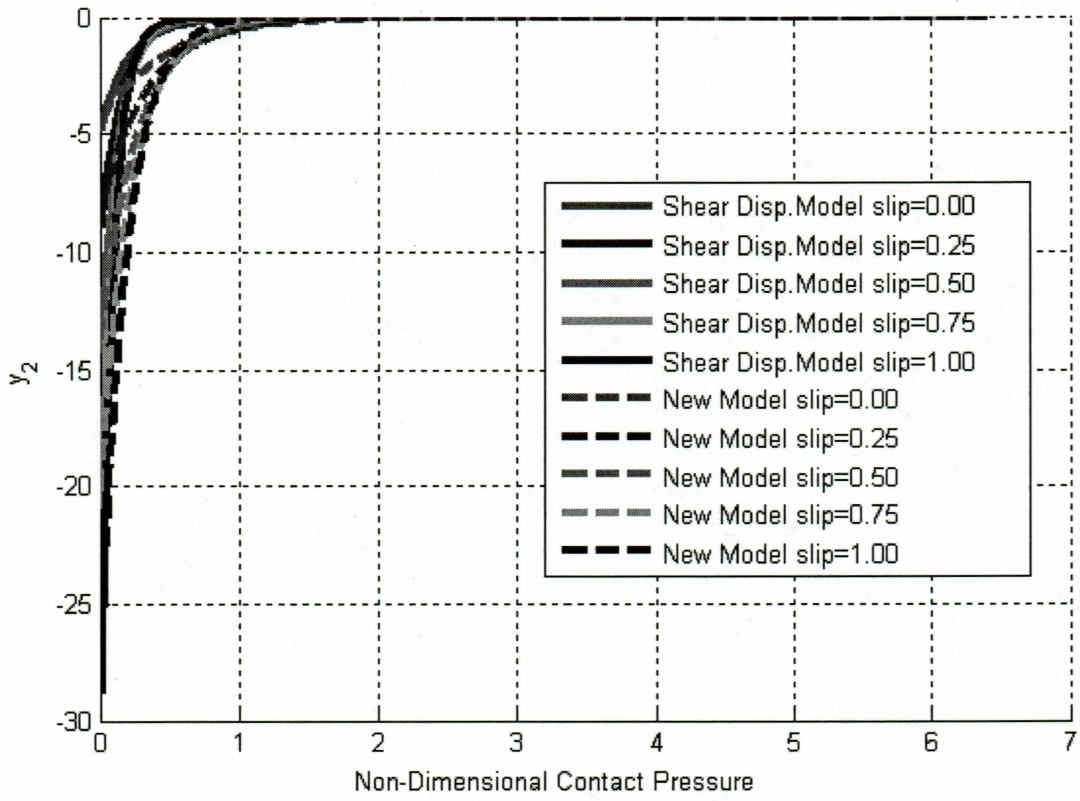

Figure 4.3 Comparison of the second order derivative of both models at various slips

From Figure 4.4 we can conclude that both models match well with respect to the following points:

- y_3 *vs.* i is always in the positive region.
- As the normal pressure increases from 0 to a small value, y_3 increases from zero to the peak value. In this case the peak value of the existing model is slightly higher than that of the new model.
- From a certain value of pressure, as the normal pressure increases y_2 is always zero.
- As the slip increases the initial slope increases for both models, and then after reaching a certain value they remain zero irrespective of the change in the slip.

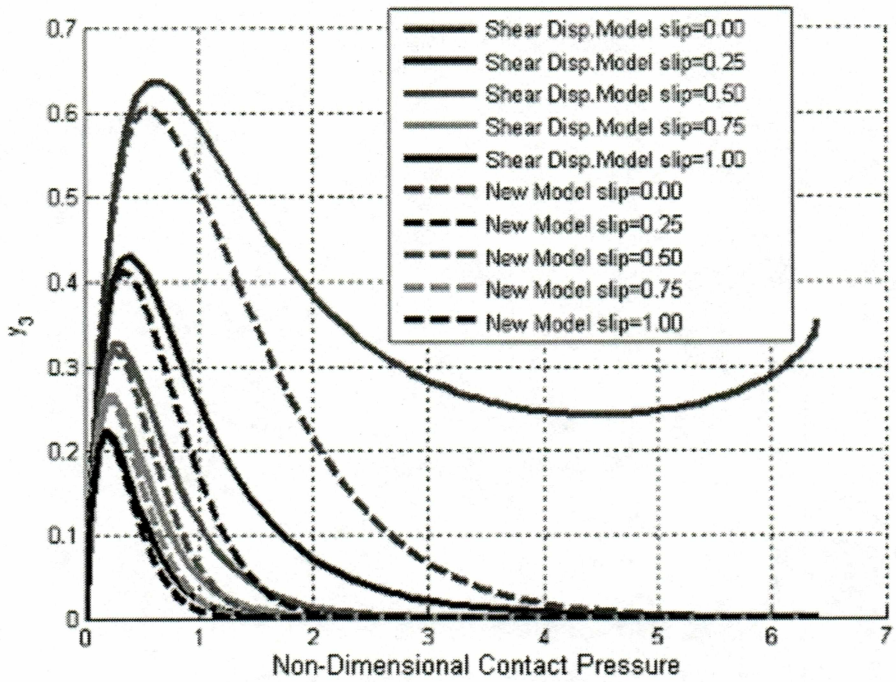

Figure 4.4 Comparison of the first order derivative of both models at various slips

From Figure 4.5 we can conclude that both models match well with respect to the following points:

- y_4 *vs* $\overline{\sigma}_n$ is always in the negative region.
- As the normal pressure increases from 0 to a small value, y_4 increases from zero to the peak value. In this case the peak value of the existing model is slightly higher than that of the new model.
- From a certain value of pressure, as the normal pressure increases y_4 is always zero.
- As the slip increases the initial slope increases for both models, and then after reaching a certain value they remain zero irrespective of the change in the slip.

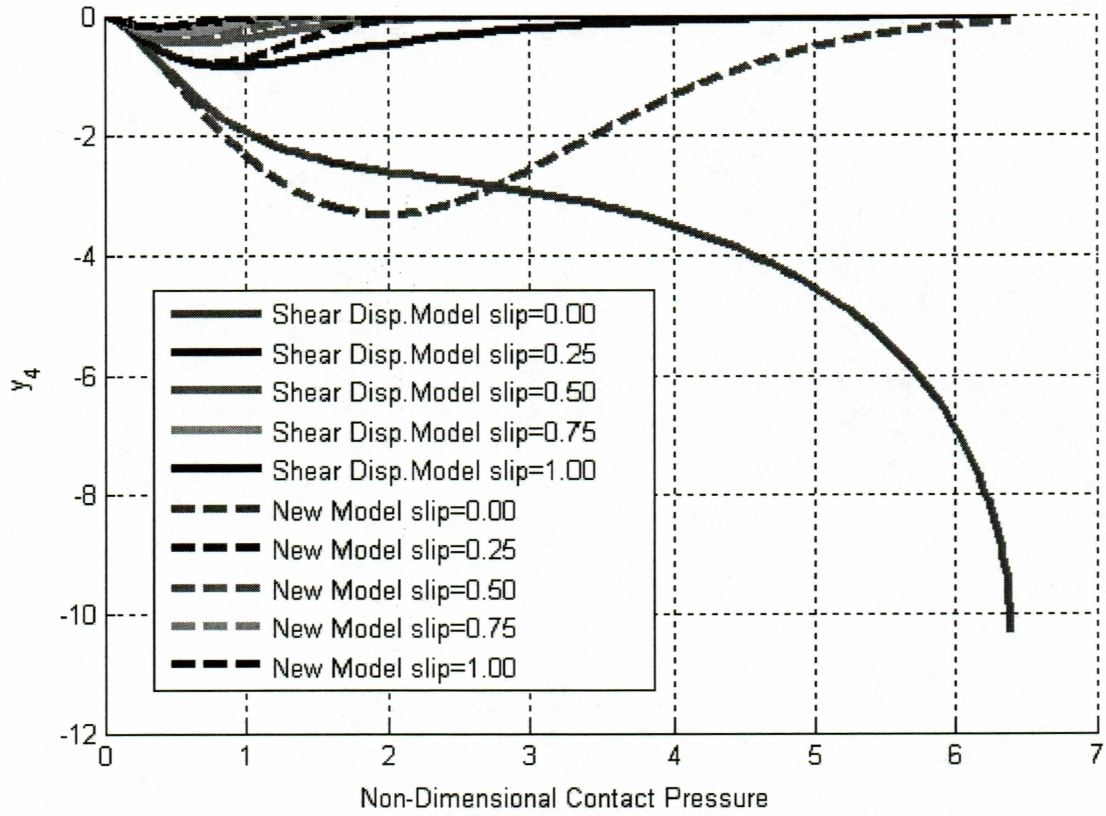

Figure 4.5 Comparison of the second order derivative of both models at various slips

The Figure 4.6 is $\overline{\tau_x}$ *vs.* $\overline{\sigma_n}$, a comparison of the resultant shear stress of Figures 4.2, 4.3, 4.4 and 4.5 with respect to the trend and order of magnitude. We can observe the following points:

- Both models almost match in trend and order of magnitude.
- Both models have positive slope, and as the slip increases the slope of the curves increases.
- After reaching a certain value of pressure, the slopes of the curves have a decreasing trend, as the second derivatives of the curves are negative.

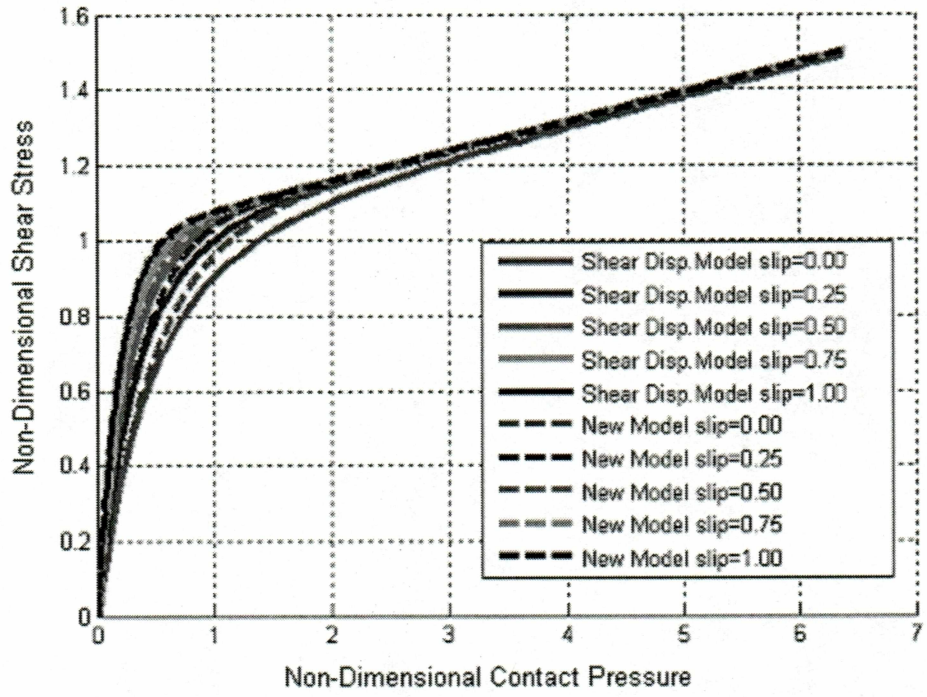

Figure 4.6 Comparison of both models at various slips

4.4 Evaluation of sinkage using Wong's equation

From Figure 4.1 the load acting on the wheel is the summation of the vertical components of the shear stress and the normal pressure, given by the equation [4]:

$$F_z - rb\left[\int_0^{\theta_0} \sigma_n \cos\theta \, d\theta + \int_0^{\theta_0} \tau_x \sin\theta \, d\theta\right] = 0 \qquad (4.14)$$

Where:

F_z - normal load

r- radius of the wheel

b - wheel width

σ_n -normal pressure

τ_x -shear stress

θ_0 -maximum contact angle

In the equation (4.14) σ_n is a function of θ, and τ_x is a function of both θ and i. Thus for every i, if we numerically integrate the equation (4.14), we get θ_0. From θ_0 we can calculate sinkage z_0 from equation (4.15).

$$z_0 = \frac{D}{2}(1-\cos\theta_0) \tag{4.15}$$

Thus the sinkage z_0 is dependent on slip (i). From Figure (4.8) we can make the following observations:

(i) All four models, the developed model, shear-displacement model [1,7, 14], upper-bound method [36], and FEA data [31] match well with each other and all the models are functions of slip.

(ii) The straight-line portion of the curve indicates that sinkage is calculated by taking shear stress as zero in equation (4.14). Thus the sinkage is independent of slip in this case.

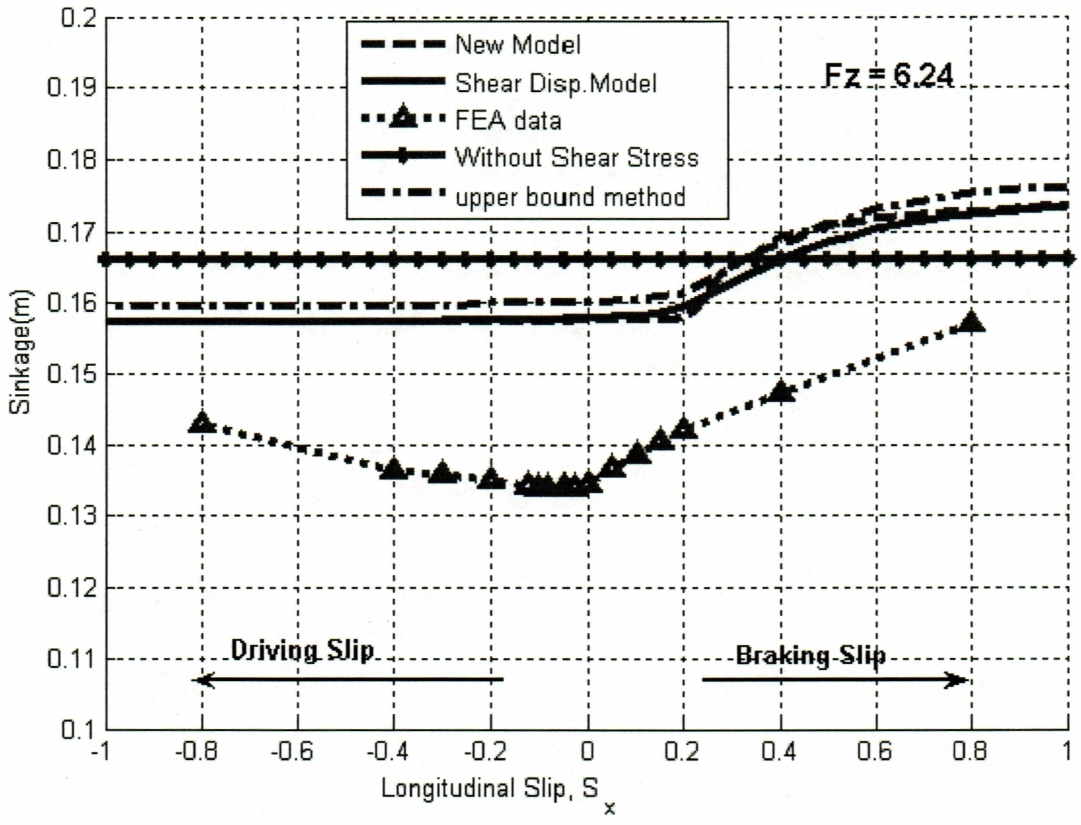

Figure 4.7 Comparison of the models in sinkage vs. slip curves

4.5 Motion Resistance

As the vehicle moves through the snow, it must overcome the resistance at each wheel caused by the snow deformation to maintain forward motion. This resistance is termed 'Motion Resistance'.

Longitudinal Motion Resistance is given by equation [4]

$$R_x = \frac{bD}{2}\int_0^{\theta_0} \sigma_n \sin\theta d\theta \tag{4.16}$$

θ_0 is a function of i as described by equation 4.14; therefore the motion resistance is also a function of i. From Figure 4.8 we can make the following observations:

(i) The predicted values of the developed shear model and the shear displacement model match well with the FEA data.

(ii) From Figure 4.8 we can see that the curve calculated without shear stress indicates no effect of slip on motion resistance, because shear stress is assumed to be zero in the sinkage calculation.

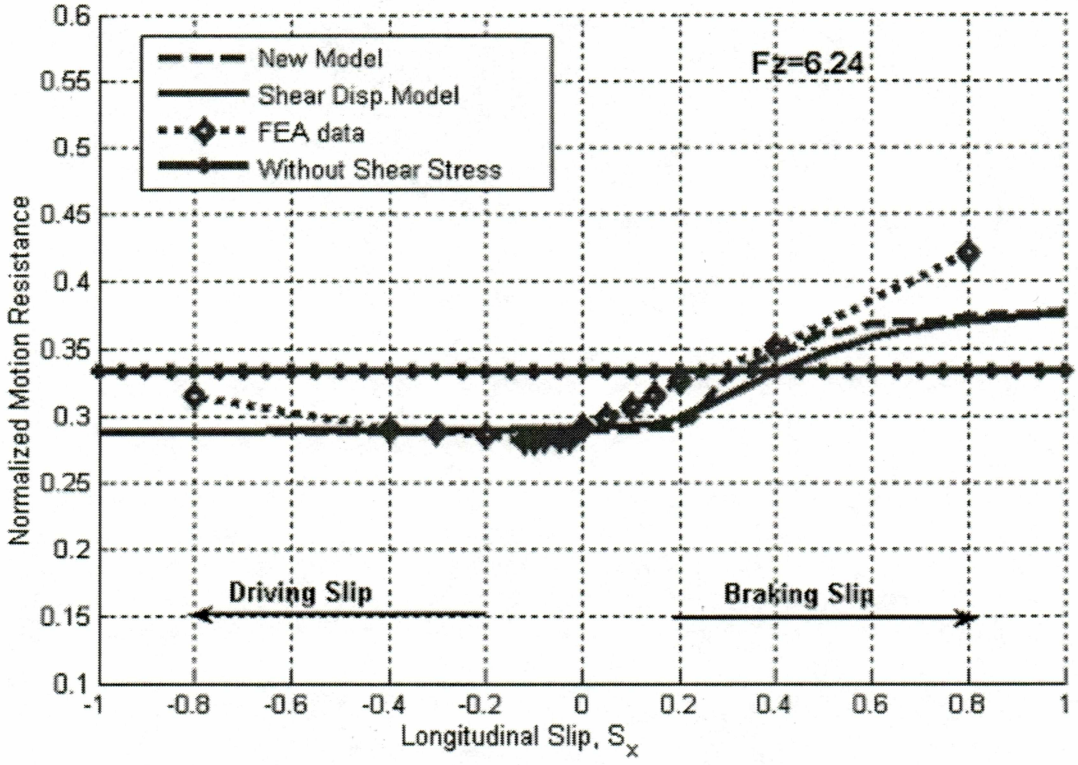

Figure 4.8 Effect of sinkage on motion resistance vs. slip.

4.6 Summary

In this chapter we developed a new semi-analytical shear stress model, in which the shear stress is function of normal load and slip at the tire/terrain interface. The calculated sinkage and motion resistance for different loads and slip using this model match well with calculation results obtained from the existing classic shear displacement model [1,7,14], FEA data [27], and the upper bound method [26].

5.Conclusions and Future Work

5.1 Conclusions

Following are the conclusion based on accomplishments during the study.

- A simplified shear stress model is developed to simulate tire/snow interaction as a function of normal pressure and slip.
- The motivation to develop this model is that it only requires normal load and slip as the inputs, eliminating the other terrain parameters such as cohesion, internal friction angle, and shear modulus which are used in existing models, and outputs the interaction forces such as the traction force, motion resistance and the draw-bar pull.
- The other advantage is the reduction in the computational time, which makes the model more appropriate for real time vehicle simulations.
- The motion resistance calculated by applying the present model is slip dependent, whereas motion resistance calculated by the existing models does not depend on slip, and may not match the real physical phenomenon of the tire/terrain interaction.
- The motion resistance calculated by the developed model, existing shear displacement model and the FEA model matched reasonably well with respect to trend and order of magnitude.
- The shear force model parameters, including tire stiffness, friction coefficients and contact pressure constants, are expressed as functions of normal load, slip (longitudinal) or slip angle (lateral) and material property parameters. Since the material properties are simple functions of loads, the computation time has been greatly reduced in comparison with the performance of the existing shear force model.
- The values of the coefficients used in the material property functions in the shear force equation are found through curve fitting using FEA data.
- The empirical equations for tire stiffness, friction coefficient and contact pressure constant were compared with FEA data and matched reasonably well.

- Shear force at the tire/terrain interface was numerically computed for pure and combined slip conditions and comparison studies were done for different turning maneuvers of the vehicle, in which the pure shear force is always greater than the combined force.

5.2 Future Work

- The present semi-analytical shear stress model could be refined further to minimize the number of tire/ snow constants, so that the computational time could be further reduced during real time simulations.
- The model should be further simplified so that the symbolic method is used to obtain the interfacial forces rather than numerical integration, which is presently used.
- In the present work only homogeneous fresh snow has been considered. The present model should be extended to non-homogeneous snow having different layers in order to be more useful in practical applications.

References

1. Wong, J. Y., "*Terramechanics and Off-Road Vehicles*", Amsterdam, The Netherlands, Elsevier Science Publishing B. V., 1989.

2. Bekker, M. G., "*Theory of Land Locomotion*", Ann Arbor, MI, University of Michigan Press, 1960.

3. William, L. H., "Vehicle Performance Over Snow", Technical Report 268, December 1975.

4. Wong, J. Y., "*Theory of Ground Vehicles*", Wiley-Interscience, 2001.

5. Shoop, S. A., "Finite Element Modeling of Tire-Terrain Interaction", Technical Report, ERDC/CRREL TR-01-16, November 2001.

6. Saarilahti, M., "Soil Interaction Model", University of Helsinki, Department of Forest Resource Management, Appendix Report No.2, May 2002.

7. Bekker, M. G., "*Introduction to Terrain-Vehicle Systems*", Ann Arbor, MI, University of Michigan Press, 1960.

8. Wong, J. Y., "Evaluation of Soil Strength Measurement", Report No. NRCC 22881, Division of Energy, National Research Council of Canada, 1983.

9. Wong, J. Y. and Preston-Thomas, J., "On the Characterization of Pressure-Sinkage Relationship of Snow Covers Containing an Ice Layer", *Journal of Terramechanics*, Vol. 20, No. 1, pp. 1-12, 1983.

10. Wong, J. Y. and Irwin, G. J., "Measurement and Characterization of Pressure-Sinkage Data for Snow Obtained Using a Rammsonde", *Journal of Terramechanics*, Vol. 29, No. 2, pp. 265-280, 1992.

11. Reece, A. R., "Principles of Soil-Vehicle Mechanics", *In Proc. Institution of Mechanical Engineers*, Vol. 180, Part 2A, 1965-66.

12. Bodin, A., "Study of the Influence of Vehicle Parameters on Tractive Performance in Deep Snow", *Journal of Terramechanics*, Vol. 38, No. 1, pp. 47-59, 2001.

13. Osman, M. S., "The Mechanics of Soil Cutting Blades", *Journal of Agricultural Engineering Research*, Vol. 6, No. 4, pp. 98, 1969.

14. Shmulevich, I., Mussel, U. and Wolf, D., "The Effect of Velocity on Rigid Wheel Performance", *Journal of Terramechanics*, Vol. 35, No. 3, pp. 189-207, 1998.

15. Wong, J. Y., and Reece, A. R., "Prediction of Rigid Wheel Performance Based on the Analysis of Soil-Wheel Stresses, Part I and part II", *Journal of Terramechanics*, Vol. 4, No .1 and 2, pp. 4, 1967.

16. Wong, J. Y., Preston–Thomas, J., "On the Characterization of the Shear Stress Displacement Relationship of Terrain", *Journal of Terramechanics*, Vol. 19, No. 4, pp.225-234, 1983.

17. Janosi, Z., Hanamoto, B., "The Analytical Determination of Drawbar Pull as a Function of Slip for Tracked Vehicles in Deformation Soils", *Int. Conf. of ISTVS,* Turin, 1961.

18. Haueisen, B., "Mobility Analysis of Small Light Weight Robotic Vehicles", Project Report, April 25, 2003.

19. "Off-Road Vehicle Mobility Evaluation", SAE J939, *Society of Automotive Engineers*, 1967.

20. Maclaurin, E. B., " The Use of Mobility Numbers to Predict the Tractive Performance of Wheeled and Tracked Vehicles in Soft Cohesive Soils", *Proceedings of the 7th European ISTVS Conference*, Ferrara, Italy, 8-10, pp. 391-398, October 1997.

21. Wismer, R. D. and Luth, H. J., "Off–Road Traction Prediction for Wheeled vehicles", *Transaction ASAE*, Vol.17, No.1, pp.8-10, 14, 1973.

22. Freitag, D. R., "A Dimensional Analysis of the Performance of Pneumatic Tires on Soft Soils", US Army Waterways Experiment Station, Report No. 3-688, 1965.

23. Rowland, D., "Tracked Vehicle Ground Pressure and Effect on Soft Ground Performance", *Proceedings of the 4th International ISTVS Conference*, Stockolm-Kiruna, Sweden, pp.353-384, April 24-28, 1972.

24. Brixius, W. W., "Traction Prediction Equations for Bias Ply Tires", ASAE Paper No 87-1622, pp.31, 1987.

25. Turnage, G. W., "Using Dimensionless Prediction Terms to Describe Off-Road Wheel Vehicle Performance", ASAE Paper No. 72-634, 1972.

26. Maclaurin, E. B., "The Use of Mobility Number to Describe the In-Field Tractive Performance of Pneumatic Tyres", *Proceedings of the 10th International ISTVS Conference*, Kobe, Japan, August 20-24, 1990.

27. Sharma, K. A. and Pandey, K. P., "Traction Data Analysis in Reference to a Unique Zero Condition", *Journal of Terramechanics*, Vol.35, No.3, pp.79-188, 1998.

28. Rowland, D. and Peel, J. W., "Soft Ground Performance Predictions and Assessment for Wheeled and Tracked Vehicles", Institute of Mechanical Engineering, pp.205, 1981.

29. Ashmore, C., Burt, C. and Turner, J., "An Empirical Equation for Predicting Tractive Performance of Log-Skidder Tyres", *Transactions of the ASAE*, Vol.30, No.5, pp.1231-1236, 1987.

30. Abd El-Gawwad, K. A. and Crolla, D. A., "Off- Road Tire Modeling 4:Extended Treatment of the Tire Terrain Interaction for Multi Spoke Model", *Journal of Terramechanics*, Vol. 36, pp. 77 –90, 1999.

31. Abd El-Gawwad, K. A. and Crolla, D. A., "Off- Road Tire Modeling 2: Effect of Camber on Tyre Performance", *Journal of Terramechanics*, Vol. 36, pp. 25 –38, 1999.

32. Abd El-Gawwad, K. A. and Crolla, D. A., "Off- Road Tire Modeling 1: The Multi Spoke Tyre Model Modified to Include the Effect of Straight Lugs", *Journal of Terramechanics*, Vol. 36, pp. 3 –24, 1999.

33. Abd El-Gawwad, K. A. and Crolla, D. A., "Off- Road Tire Modeling 3: Effect of Angled Lugs on Tyre Performance", *Journal of Terramechanics*, Vol. 36, pp. 63 –75, 1999.

34. Nakajima, Y., "Analytical Model of Longitudinal Tire Traction In Snow", *Journal of Terramechanics*, Vol. 40, pp. 63-82, 2003.

35. Janosi, Z., Hanamoto, B., "The Analytical Determination of Drawbar Pull as a Function of Slip for Tracked Vehicles in Deformation Soils", *Int. Conf. of ISTVS*, Turin, 1961.

36. Blaisdell, G. L., Richmond P. W., Shoop, S. A., Green, C. E., and Alger, R. G., "Wheels and Tracks in Snow: Validation Study of the CRREL Shallow Snow Mobility Model", USA Cold Regions Research and Engineering Laboratory, CRREL Report 90-9.

37. Richmond P. W., "Motion Resistance of Wheeled Vehicles in Snow", USA Cold Regions Research and Engineering Laboratory, CRREL Report 90-9.

38. Lang, T. E. and Dent, J. D., "Review of Surface Friction, Surface Resistance, and Flow of Snow", *Reviews of Geophysics and Space Physics*, Vol. 20, No. 1, Pages 21-37, February 1982.

39. Wong, J.Y., "Behaviour of Soil Beneath Rigid Wheel", *Proc, 2nd Int. Conf. of the International Society for Terrain Vehicle Systems*, Toronto, Canada, University of Toronto Press, 1966.

40. Van Es, G. W. H., "Methods for Prediction of Rolling Resistance of Air Craft Tyres in Dry Snow", *Journal of Aircraft*, Vol.36, No.5, pp. 762-768, 1999.

41. Crolla, D. A and Razaz, A. S. A., "A Review of the Combined Lateral and Longitudinal Force Generation of Tires on Deformable Surfaces", *Journal of Terramechanics*, Vol. 24, No. 3, pp.199-225, 1987.

42. Zhang, T. and Lee, J. H., "Finite Element Method Simulation of the Interaction Between a Deformable Tire and Snow", *Proceedings of the 7th Asia-Pacific Conference and the 25th Annual Meeting of the Japanese Society for Terramechanics of the ISTVS*, Changchun, China, 2004.

43. Bakker, E., Nyborg, L. and Pacejka, H. B., "Tyre Modelling for Use in Vehicle Dynamics Studies", *SAE Technical Paper Series, International Congress and Exposition*, Detroit, Michigan, February 23-27, 1987.

44. Lacombe, J., "Tire Model for Simulations of Vehicle Motion on High and Low Friction Road Surfaces", *Proceedings of the 2000 Winter Simulations Conference*, Orlando, Florida, 2000, pp.1025-1034.

45. Segel, L., "The Mechanics of Heavy Duty Trucks and Truck Combinations", Presented at the Engineering Summer Conference, University of Michigan, Ann Arbor, 1984.

46. Guo, K. and Sui, J., "Theoritical Observation on Emperical Expression of Tire Shear Forces", *Proceedings of the 1995 14th IAVSD Symposium on the Dynamics of Vehicles on Roads and Tracks*, Ann Arbor, Michigan, 1995.

47. Iagnemma, Karl and Dubowsky, S., "Terrain estimation for high-speed rough-terrain autonomous vehicle navigation", *Unmanned Ground Vehicle Technology IV*, SPIE Conference Proceedings, April 2002

48. Tatsuro, M., "Tractive Performance of a Driven Rigid Wheel on Soft Ground Based on the Analysis of Soil-Wheel Interaction", *Journal of Terramechanics*, Vol. 30, No. 5, pp. 351-369, 1993.

49. Shikanai, T., Hashiguchi, K., Nohse, Y., Ueno, M. and Okayasu, T., "Precise Measurement of Soil Deformation and Fluctuation in Drawbar Pull for Steel and Rubber-Coated Rigid Wheels", *Journal of Terramechanics*, Vol. 37, pp. 21-39, 2000.

50. Vechinski, C. R., Johnson, C. E. and Raper, R. L., "Evaluation of an Empirical Traction Equation for Forestry Tires", *Journal of Terramechanics*, Vol. 35, No. 1, pp. 55-57, 1998.

51. Wulfsohn, D. and Upadhyaya, S. K., "Traction of Low-Pressure Pneumatic Tires in Deformable Terrain", *SAE Technical Paper Series*, International Off-Highway and Powerplant Congress and Exposition, Milwaukee, Wisconsin, September 9-12, 1991.

52. Upadhyaya, S. K., Wulfsohn, D. and Mehlschau, J., "An Instrumented Device to Obtain Traction Related Parameters", *The American Society of Agricultural Engineers*, Hyatt Regency Columbus at Ohio Center, Columbus, Ohio, June 24-27, 1990

53. Lee, J. H., "Upper Bound Analysis of Upsetting of Pressure-Sensitive Polymeric Rings", *International Journal of Mechanical Sciences*, Vol.30, No.8, 1988, pp.601-612.

Appendix

Step 1 The non-dimensional shear displacement equation is given by

$$\bar{\tau}_x = \left(1 + \bar{\sigma}_n \tan\phi\right)\left(1 - \frac{J_k}{u_k}\right)$$

$$J_k = u_k \exp\left(-u_k J\right)$$

$$\bar{\sigma}_n = \left(\frac{p_w}{c}\right)\left(-\ln Z\right) \qquad \text{or} \qquad Z = \exp\left[-\left(\frac{c}{p_w}\right)\bar{\sigma}_n\right]$$

$$Z = 1 - \frac{1}{2}\left(\frac{D}{z_w}\right)\left(\cos\theta - \cos\theta_0\right)$$

$$J = \frac{1}{2}\left[\left(\theta_0 - \theta\right) - \left(1 - i\right)\left(\sin\theta_0 - \sin\theta\right)\right]$$

Step 2 The definitions used for simplification are given below

$$T_0 = Z\left(\frac{z_w}{D}\right)\left(\frac{c}{p_w}\right) \qquad Q_0 = J_k\left(1 + \bar{\sigma}_n \tan\phi\right)$$

$$Q_1 = \left(i\frac{\cos\theta}{\sin\theta}\right) \qquad Q_2 = \left(\frac{1 - \cos\theta}{\sin\theta}\right)$$

$$T_1 = Q_0 Q_1 \qquad T_2 = Q_0 Q_2$$

Step 3 Identities

$$\frac{\partial\theta}{\partial Z} = \frac{1}{\left(\frac{\partial Z}{\partial\theta}\right)} = \frac{1}{\frac{1}{2}\left(\frac{D}{z_w}\right)\sin\theta} = 2\left(\frac{z_w}{D}\right)\left(\frac{1}{\sin\theta}\right)$$

$$\frac{\partial Z}{\partial \bar{\sigma}_n} = \left(\frac{c}{p_w}\right)\exp\left[\left(\frac{c}{p_w}\right)\bar{\sigma}_n\right] = \left(\frac{c}{p_w}\right)Z$$